Magnetic Resonance Imaging Based Quantification of Ophthalmic Adaptations to Microgravity and Microgravity Analogs

A Thesis

Presented in Partial Fulfillment of the Requirements for the

Degree of Master of Science

with a

Major in Biological Engineering

in the

College of Graduate Studies

University of Idaho

by

Stuart H. Sater

Major Professor: Dev Shrestha, Ph.D.

Committee Members: Bryn Martin, Ph.D., Nathen Schiele, Ph.D.

Department Administrator: Ching-An Peng, Ph.D.

December 2020

Authorization to Submit Thesis

This thesis of Stuart Sater, submitted for the degree of Master of Science with a major in Biological engineering and titled, "Magnetic Resonance Imaging Based Quantification of Ophthalmic Adaptations to Microgravity and Microgravity Analogs," has been reviewed in final form. Permission, as indicated by the signatures and dates given below, is now granted to submit final copies to the College of Graduate Studies for approval.

Major Professor: _____ Date: _____
Dev Shrestha, Ph.D.

Committee Members: _____ Date: _____
Bryn Martin, Ph.D.

_____ Date: _____
Nathen Schiele, Ph.D.

Department Administrator: _____ Date: _____
Ching-An Peng, Ph.D.

Abstract

Spaceflight has long been known to have adverse effects on the human body. Many spaceflight-induced alterations such as bone and muscle atrophy are well understood and have mitigation strategies that have been successfully implemented. More recently, some astronauts have been presenting with a series of unusual physiologic and pathologic neuro-ophthalmic symptoms after long-duration spaceflight (> 6 months). These symptoms are collectively referred to as Spaceflight Associated Neuro-Ocular Syndrome (SANS), and include optic disc edema, posterior optic globe flattening, retinal and choroidal folds, cotton wool spots, and hyperopic refractive error shift. SANS is thought to be caused in part by mild but chronic elevation in intracranial pressure (ICP) caused by a headward fluid redistribution that occurs in space due to the lack of a gravitational vector. To simulate these headward fluid distributions, head-down tilt (HDT) studies have been implemented as a ground-based analog to spaceflight. HDT studies are advantageous in that they offer more opportunities to test mitigation techniques, more comprehensive imaging and monitoring, and allow for a larger number of study subjects in a shorter amount of time. The following studies provide automated and quantitative assessment of physiologic neuro-ophthalmic changes that occur due to spaceflight and HDT. Optic nerve (ON) and optic nerve sheath (ONS) cross sectional areas and ON deviation were assessed in healthy subjects during acute head-down tilt. While ON area did not change, both ONS area and ON deviation increased significantly. The posterior globes of long-duration spaceflight astronauts and HDT subjects were quantitatively assessed for globe flattening in the form of posterior volume displacement. Both cohorts reported significant volume displacement that in the case of astronauts did not resolve within a year after landing. Furthermore, centrifugation was tested as a mitigation technique for globe flattening in the HDT cohort and was not found to significantly

reduce volume displacement. The quantitative methods described here will help in the understanding of SANS etiology and will inform future mitigation strategies.

Acknowledgments

I would like to thank Dr. Martin for mentoring me throughout this project and for providing me the opportunity to contribute to this incredible field. Through his support I have been able to learn and accomplish things beyond my imagination. I would also like to thank Dr. Shrestha for taking on this project and helping me to carry it through to its current state. His mentorship in my education and developing the work presented here will be invaluable for my future endeavors. Additionally, I would like to thank Dr. Schiele for his guidance and expertise throughout my educational career and for providing crucial feedback in the development of my thesis. I would like to thank Dr. Ethier, Dr. Marshell-Goebel, Dr. Macias, and all other collaborators and co-authors for the knowledge and feedback they provided. Their mentorship helped me to become a better writer, investigator, and critical thinker. Finally, I would like to thank the astronauts who risk their lives and provide invaluable data to the scientific community by completing experiments and subjecting themselves to the endless barrage of medical tests and imaging that make these studies possible.

Dedication

I would like to thank my friends and family for supporting me throughout my life. I want to thank my father, Jeff, for fostering a curiosity for understanding how things work, and my mother, Wendy, for instilling me with the work ethic I have today. Finally, I want to thank my wife, Shelby, who has always been by my side and has helped and supported me throughout my educational endeavors.

Table of Contents

List of Figures

List of Tables

Statement of Contribution

Bryn Martin conceived of the presented idea and secured research funding for the work. Stuart Sater led publication of manuscripts overall presentation of results. Stuart Sater Jesse Rohr, Austin Sass, and Bryn Martin developed the theory. Stuart Sater, Austin Sass, Gabryel Conley Natividad, and Jesse Rohr developed and scripted measurement parameters. Stuart Sater, Austin Sass, Gabryel Conley Natividad, Akari Seiner and Jesse Rohr performed analysis of measurements and assisted in drafting manuscripts and figures. All authors provided critical feedback and commented on the manuscript.

Authors:

Stuart Sater: Neurophysiological Imaging and Modeling Laboratory

University of Idaho, Moscow, ID

Austin Sass: Neurophysiological Imaging and Modeling Laboratory

University of Idaho, Moscow, ID

Akari Seiner: Neurophysiological Imaging and Modeling Laboratory

University of Idaho, Moscow, ID

Jesse Rohr: Neurophysiological Imaging and Modeling Laboratory

University of Idaho, Moscow, ID

Gabryel Conley Natividad: Neurophysiological Imaging and Modeling Laboratory

University of Idaho, Moscow, ID

Karina Marshall Goebel: Johnson Space Center Cardiovascular and Vision Laboratory

KBR, Houston, TX

C. Ross Ethier: Wallace H. Coulter Department of Biomedical Engineering

Georgia Institute of Technology and Emory University, Atlanta, GA

Michael B. Stenger: Johnson Space Center Cardiovascular and Vision Laboratory

National Aeronautics and Space Administration, Houston, TX

Eric M. Bershad: Department of Neurology

Baylor College of Medicine, Houston, TX

Brandon Macias: Johnson Space Center Cardiovascular and Vision Laboratory,

KBR, Houston, TX

Dev Shrestha: Department of Chemical and Biological Engineering,

University of Idaho, Moscow, ID

Bryn A. Martin: Alcyone Therapeutics

Lowell, MA

Chapter 1: Background

Spaceflight has been known to result in a series of negative effects on the human body. Some of these effects are well-documented and have mitigation techniques that are well-established, including musculoskeletal deconditioning and resistive exercise. However, as longer-duration spaceflight missions have become more common, other health issues related to spaceflight have come to light. The National Aeronautics and Space Administration (NASA) Human research Program (HRP) has composed a roadmap that shows the severity of various spaceflight-associated risks and a timeline for when these risks should be assessed and mitigated (Figure 1.1)[1].

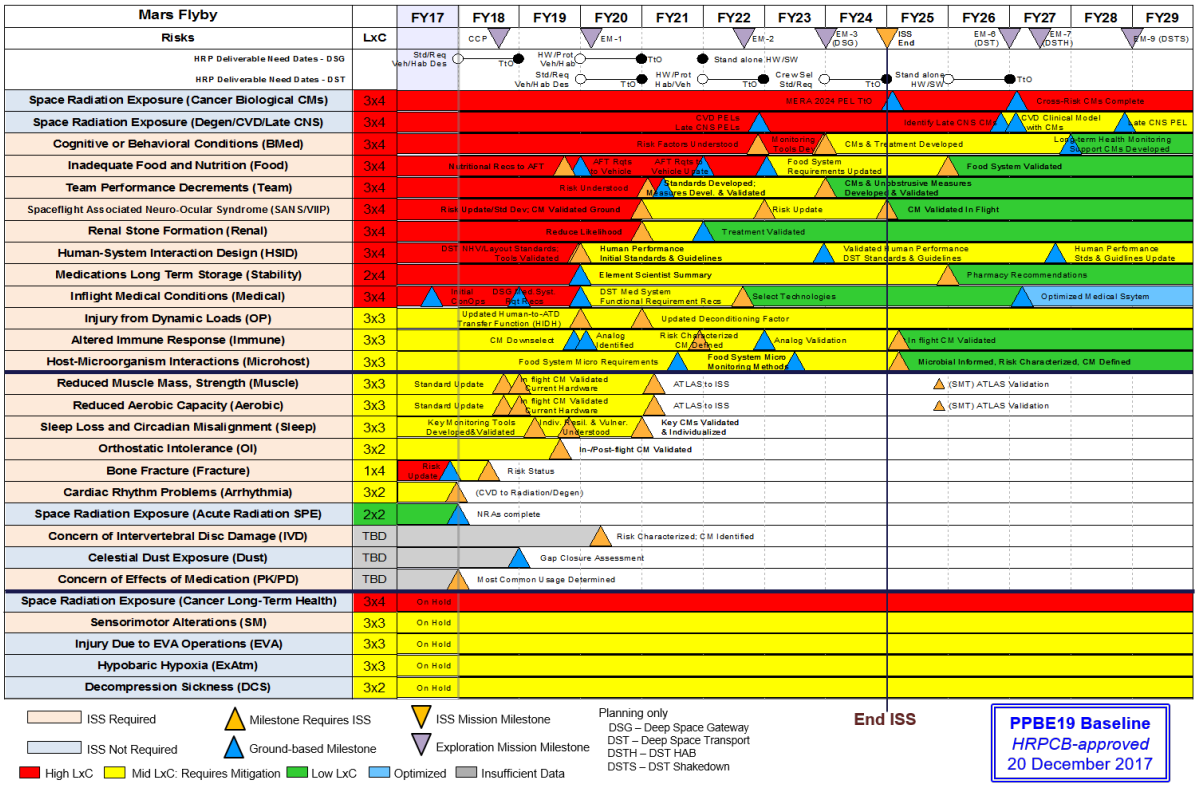

Figure 1.1 NASA HRP integrated path to risk reduction highlighting all current risks associated with long-duration spaceflight missions[1].

Spaceflight Associated Neuro-Ocular Syndrome

One of the more significant risks identified in the human research roadmap is Spaceflight Associated Neuro-Ocular Syndrome (SANS) which can cause reduced visual acuity during and after spaceflight. SANS is typically attributed to long-duration spaceflight missions (>six months) which have only recently been possible with the success of the International Space Station (ISS). The proportion of astronauts who are diagnosed with SANS is about 40 percent, but varies over time due to the ongoing characterization of its formal designation[2,3]. The underlying etiology of SANS is currently unknown, but it is hypothesized that a cephalad fluid redistribution that occurs in the absence of a gravitational vector is a contributor to ophthalmic alterations (Figure 1.2). These fluid redistributions are thought to result in mildly elevated intracranial pressure (ICP) that can lead to optic disc edema, posterior optic globe flattening, retinal and choroidal folds, cotton wool spots, and hyperopic refractive error shift[2]. These symptoms likely become more severe with spaceflight duration and have been shown to persist beyond seven years postflight[4]. A more comprehensive understanding of SANS and development of effective mitigation techniques are necessary before interplanetary and extended-duration spaceflight missions are possible.

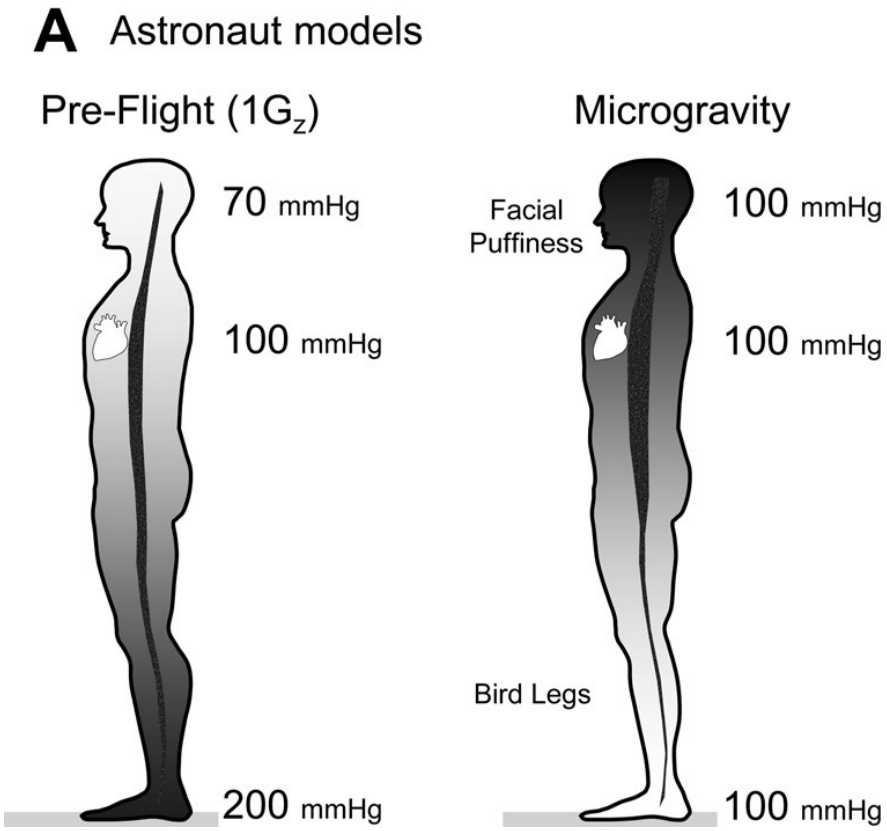

Figure 1.2 Adaptive responses to fluid redistributions in the absence of a gravity include facial puffiness, bird legs, and arterial pressure changes (mmHg). Dark shades indicate more tissue fluid[5].

Intracranial Pressure

SANS was formally known as visual impairment intracranial pressure (VIIP) syndrome, which reflects the original hypothesized etiology that ICP was significantly elevated during spaceflight. This is because SANS shares some symptomology with idiopathic intracranial hypertension (IIH), including globe flattening, cotton wool spots, choroidal folds, and optic disc edema. However, optic disc edema is usually bilateral in IIH and unilateral in SANS, and the classic symptoms of IIH (chronic headache, pulse synchronous tinnitus, and diplopia) are completely absent in SANS[6]. This has led researchers to suspect that intracranial pressure may not be pathologically elevated and that other contributing factors are involved. This suspicion

has been supported by supine-level lumbar opening pressures (LBOP) in astronauts with SANS[4] and the absence of optic nerve sheath (ONS) distension after long-duration spaceflight[7]. Even if ICP is not pathologically elevated in space, it is likely elevated to supine levels and does not fluctuate with changing postures as it does on Earth. Mild elevations may also be exacerbated during resistive exercise which is speculated to generate spikes in ICP[8].

Head-down tilt (HDT) bed rest studies are currently used as ground-based spaceflight analogs because the HDT position simulates fluid redistributions and mild ICP elevation that are suspected to occur in microgravity[9]. However, the presence of a constant gravitational vector during HDT may elicit different physiological responses compared to spaceflight. A subjective assessment of ground-based spaceflight analogs found that HDT showed good fidelity in simulating the effects of microgravity for fluid redistribution but not for neurologic and pulmonary function[10].

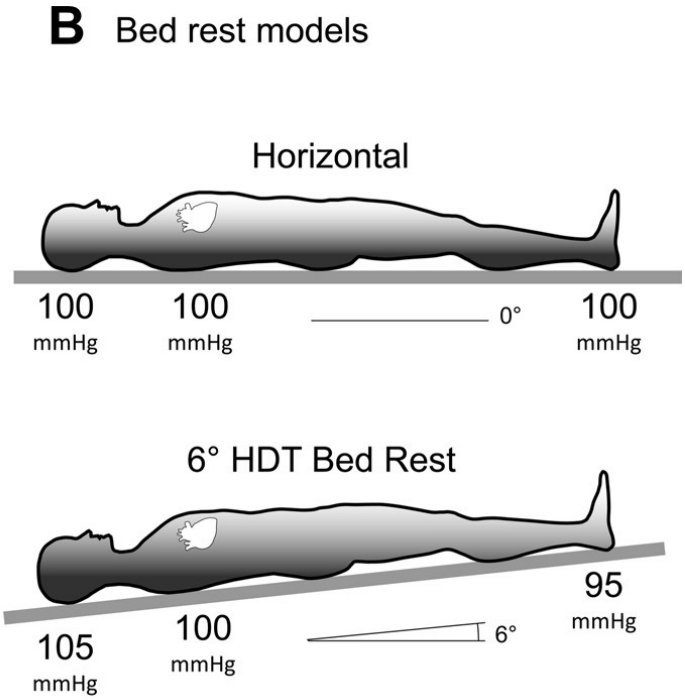

Figure 1.3 Adaptive responses to fluid redistributions in head-down-tilt, with hypothesized arterial pressure changes (mmHg). Dark shades indicate more tissue fluid[5].

SANS Symptoms

One structure that is broadly affected by spaceflight is the choroid. The choroid is a highly vascularized space between the retina and the sclera. Choroidal expansion has been identified using optical coherence tomography (OCT) and retinal photography during HDT, parabolic flight, and spaceflight. Choroidal expansion may lead to intraocular pressure (IOP) changes and other structural anomalies including choroidal folds (Figure 1.4 b,c). Choroidal folds occur when circumferential pressure exerted on the ON and have been documented years after return from space[11].

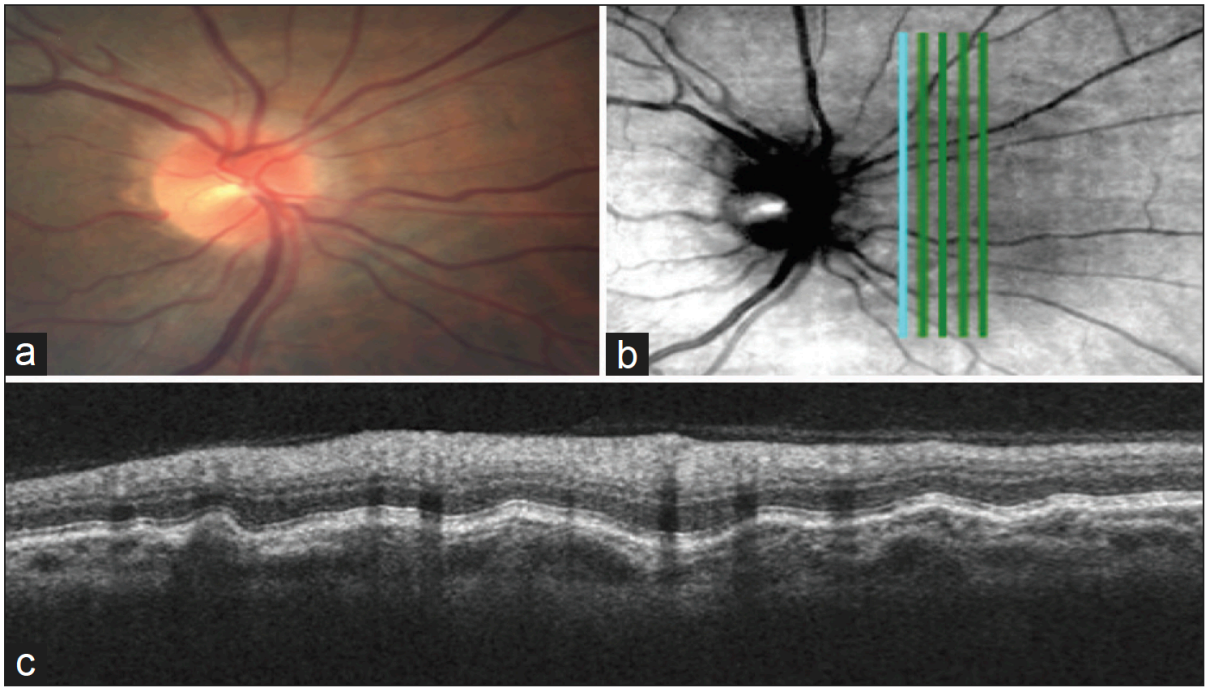

Figure 1.4 Postflight imaging of a) fundus imaging showing Frisen Grade 1 disc edema, b) choroidal folds superior and inferior to the optic disc, and c) the retinal cross-section showing retinal nerve fiber layer thickening and choroidal folds[12].

Another common symptom of SANS is optic disc edema which represents the primary diagnostic criteria for the disorder (Figure 1.4 a). The Frisen grading scale system as quantified by fundus photography is the current standard for assessing clinical disc edema. The combination of choroidal expansion and optic disc edema may contribute to globe flattening; however, globe flattening is usually more significant than what could be explained by optic disc edema and choroidal expansion alone. Thus, globe flattening is usually considered to be indicative of scleral indentation near the optic nerve head (ONH) and is thought to be caused by perineural forces at the back of the eye and/or changes in the trans-laminar pressure difference (TLPD) where ICP becomes greater than IOP (Figure 1.5)[13]. Previous studies have identified globe flattening subjectively and without preflight baselines for comparison. Robust quantitative methods are needed to accurately assess the significance of globe flattening in long-duration spaceflight.

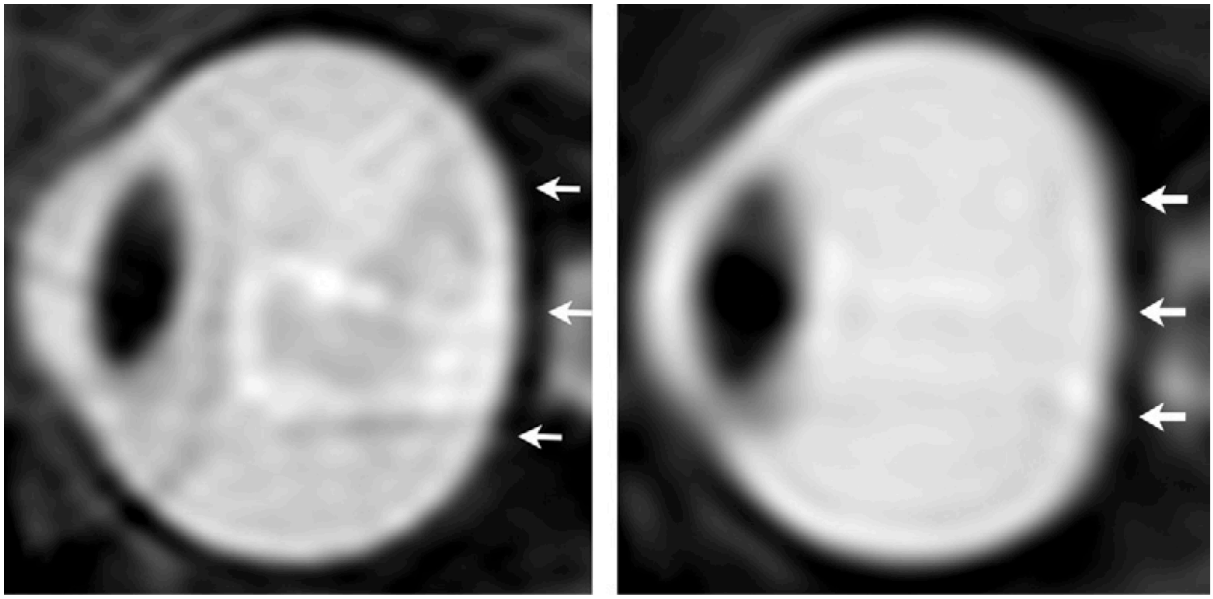

Figure 1.5 Sagittal T2 weighted MRI subjectively showing posterior globe flattening after spaceflight (right)[14].

Chapter 2: Research Objectives

The primary goal of the work presented here was to develop and apply automated methods to quantify ophthalmic adaptations to long-duration spaceflight and spaceflight analogs to better understand the underlying pathophysiology of SANS.

Specific Aim 1

To quantify changes in ON deviation, ON area, ONS area, and vitreous chamber depth in healthy subjects after 30 minutes of 15° HDT (Figure 2.1 A)

Specific Aim 2

To use pre and postflight optic globe geometries to quantify changes in posterior globe volume in astronauts after long duration spaceflight (Figure 2.1 B).

Specific Aim 3

To quantify the recovery profile of posterior optic globe volume changes in astronauts after long duration spaceflight (Figure 2.1 C).

Specific Aim 4

To quantify changes in posterior globe volume in healthy subjects during and after 60 days of strict 6° HDT bed rest (Figure 2.1 D).

Specific Aim 5

To quantify the effectiveness of centrifuge (AG) countermeasures in preventing changes in posterior globe volume during and after 60 days of strict 6° HDT bed rest (Figure 2.1 D).

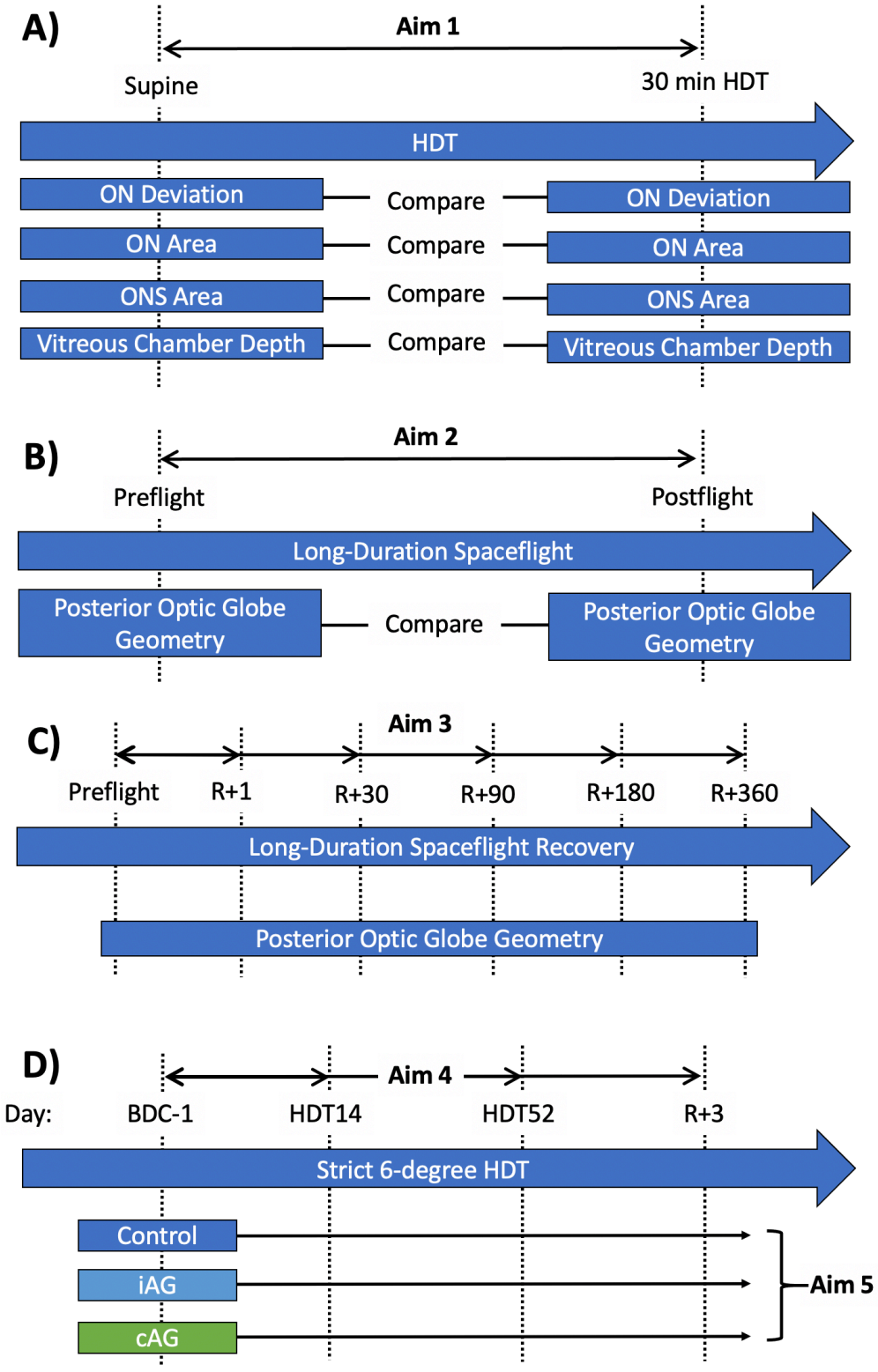

Figure 2.1 Overview of the proposed research study aims. iAG represents intermittent artificial gravity and cAG represents continuous artificial gravity.

Chapter 3: MRI Based Quantification of Ophthalmic Changes in Healthy Volunteers During Acute 15° Head-Down Tilt as an Analog to Microgravity

Forthcoming in The Journal of Royal Society Interface

Abstract

Spaceflight is known to cause ophthalmic structural and functional changes in a condition known as Spaceflight Associated Neuro-ocular Syndrome (SANS). It is hypothesized that SANS is caused by cephalad fluid shifts occurring in the absence of a gravitational vector that result in mild but chronically elevated intracranial pressure (ICP). Head-down tilt (HDT) studies are routinely implemented as a ground-based spaceflight analog to simulate the cephalad fluid shifts and elevated ICP that occur during exposure to microgravity. Non-invasive automated and manual techniques were developed and applied to magnetic resonance (MR) images to quantify changes in ophthalmic structures during acute 15° HDT and estimate Young's modulus of the optic nerve sheath (ONS). This will help our understanding of SANS and the potential role of ICP in the physiological response of ophthalmic structures. The ONS cross sectional area was found to increase by 4.10 ± 3.24 mm^2 under HDT while the optic nerve (ON) cross sectional area remained unchanged. ON deviation was also found to increase by 0.24 ± 0.38 mm an indication of increased tortuosity. A decrease in vitreous chamber depth of 0.24 ± 0.38 mm suggests that HDT may contribute to globe flattening. A thick-walled cylinder assumption of the law of Laplace was applied to estimate an ONS Young's modulus of 85.0 kPa. The presented findings support previous research showing that acute HDT alters ophthalmic structures including the ONS and provides in vivo estimations of ONS Young's modulus

Introduction

Extended spaceflight is known to result in abnormal adaptations in human physiology. For instance, musculoskeletal deconditioning and cardiovascular adaptations have been extensively studied and have pathologies that are well defined[15-18]. More recently, neuro-ocular functional and structural changes have been identified in a condition referred to as Spaceflight Associated Neuro-ocular Syndrome (SANS)[2]. Crewmembers with SANS often present with choroidal folds, hyperopic shift, posterior globe flattening, and optic disc edema[14,19,20], with optic disc edema representing the primary diagnostic criteria for the syndrome[21]. These symptoms of SANS can result in reduced visual acuity and farsightedness and can persist long after return to Earth, although some recovery has been shown to occur[22]. Furthermore, SANS represents a major risk factor for current 6-month missions to the International Space Station (ISS), requiring mitigation before long-term space habitation (1 year or more) or deep space expeditions will become feasible.

SANS pathophysiology has been studied extensively yet is not well understood[23]. A prevailing theory suggests that cephalad fluid shifts occurring in microgravity result in mild but chronically elevated intracranial pressure (ICP) that elicit adaptations of ophthalmic structures including distension of the bulbar region of the optic nerve sheath (ONS)[3,24]. Significant increases in ICP may also result in a reversal of the trans-laminar pressure gradient, wherein ICP becomes greater intraocular pressure (IOP), contributing to hyperopic shift and optic disc edema[13,25]. This hypothesis has been supported by elevated lumbar puncture opening pressures postflight[19], and similarities in symptoms between SANS and idiopathic intracranial hypertension (IIH), such as papilledema and posterior globe flattening[14]. However, some

common symptoms of IIH have not been documented in crewmembers, including chronic headache, transient visual obscurations, tinnitus, and diplopia [6]. The discrepancies between SANS and IIH suggest that the etiology of SANS cannot be explained by elevated ICP alone and is likely multifactorial, requiring further evaluation[23].

To help evaluate the role of ICP in SANS, head-down tilt (HDT) studies have been routinely implemented to simulate the headward fluid shifts experienced in weightlessness[9]. However, there is evidence suggesting that HDT overestimates the fluid shifts experienced under microgravity. Laurie et al. found an overrepresentation of optic disc edema in subjects who participated in strict 6º HDT for 30 days (45%), when compared to the prevalence in astronauts (15%)[21]. HDT studies can vary wildly in the angle of HDT, duration, and ambient environment. One study investigating the effects of HDT angle on ICP and IOP found that ICP was only significantly elevated beyond supine levels at angles of at least 18°[25]. Therefore, we utilized 15° HDT to simulate the cephalad fluid shifts suspected to occur in space.

The present study uses a novel magnetic resonance image (MRI) processing technique to quantify changes to ophthalmic structures under acute 15° HDT. We hypothesize that features of elevated ICP will manifest under HDT in the form of ONS distension and decreased vitreous chamber depth. Changes in other parameters such as optic nerve (ON) cross sectional area, ON deviation, and gaze angles were also assessed. Demographic effects were also investigated to identify possible covariates such as sex, BMI, and age. The effects of HDT recognized by this study can be compared to structural changes observed in astronauts to better understand the role of ICP in the development of SANS.

Methods

MRI data collection for this study was approved by the Georgia Institute of Technology, Emory University, and the University of Idaho institutional review boards and satisfied all local and international regulations for human subject research.

Study Design

High resolution MRI scans were collected for 18 healthy volunteers (10 males and 8 females) on a 3 Tesla MRI scanner (Prisma, Siemens Healthineers), using a 20-channel receiving coil. Each subject was scanned in a supine position followed by a 30-minute acclimation period in 15º HDT position before a second scan was taken. To minimize motion artifacts due to changes in gaze angles during MRI scans, subjects were instructed to focus on a visual target central to their field of view. Both T1 and T2 weighted MRI scans were collected to analyze the effect of HDT on the ON and ONS. Parameters were generated to analyze changes to the ON and ONS cross-sectional areas, ON deviation, optic globe, and gaze angle.

ON and ONS Cross-sectional Areas

To assess changes in cross-sectional areas of the ON and ONS, 3D geometries of these structures were generated using the following semi-automated method. High-resolution T2-weighted coronal MRI scans were collected with 600 µm slice thickness and spacing, and 253 µm in-plane isotropic pixel size (FOV 256 x 256) (Figure 3.1). Additional sequence parameters included 170° flip-angle, 820 ms repetition time, and 118 ms echo time. To extract ON and ONS contours, an adaptive thresholding process was implemented. First, average background

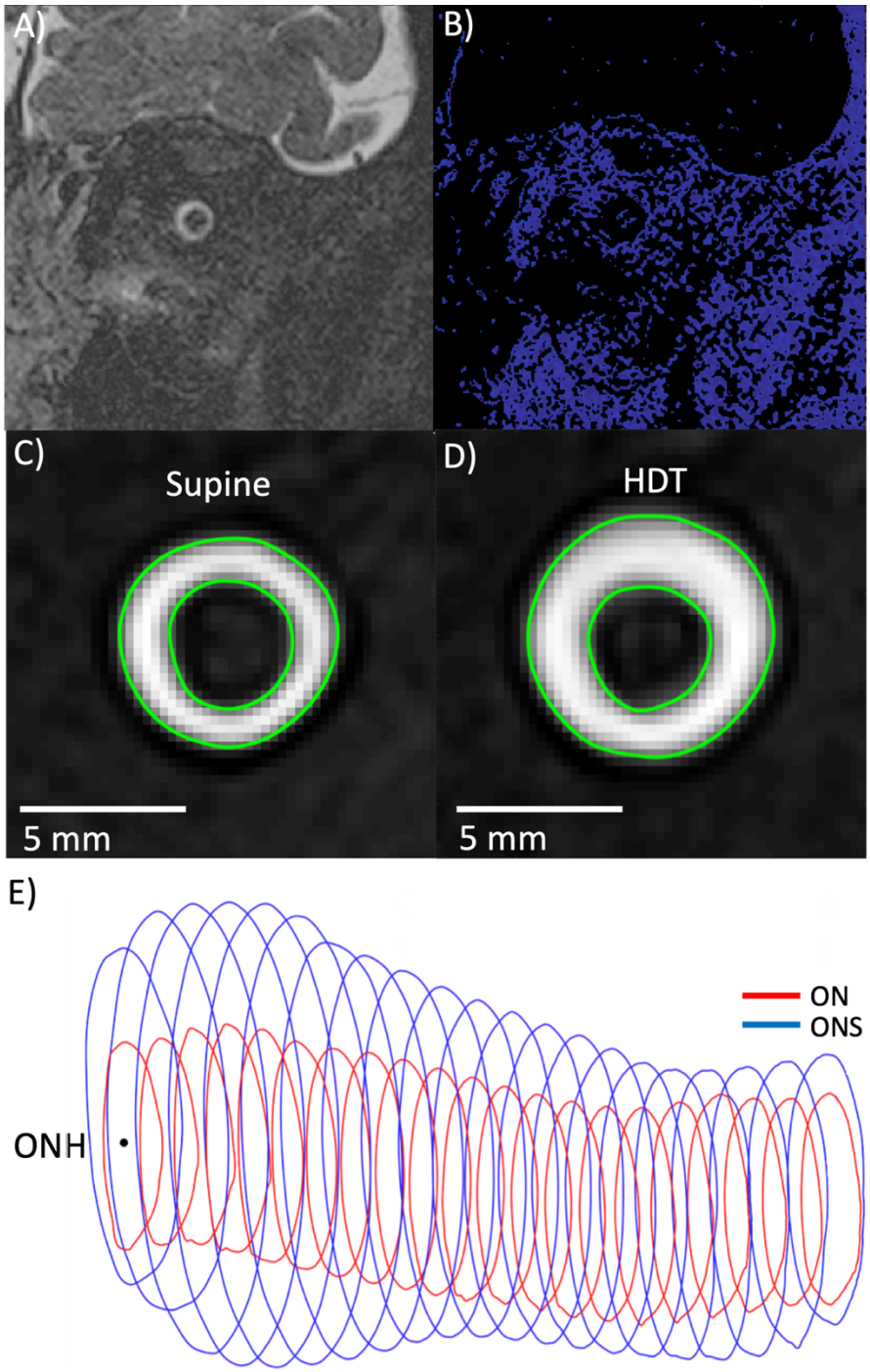

Figure 3.1. Methods for analysis of ON and ONS areas showing A) example coronal MRI before and B) after mask is applied based on histogram analysis of peak intensity values. C) Supine and D) HDT contours resulting from largest ONS area change at 3 mm location posterior to ONH (subject 16R). E) 3D representation of ON/ONS trajectory starting at the ONH showing contours at each slice of MRI volumetric data (subject 16R). Additional ONS slices that were generated using the ONS extension method are shown.

pixel intensity for each scan was selected with a slice-by-slice mask relative to the peak frequency in the pixel intensity histogram, with the intensity ranging from 0 to 4095 (12-bit image), excluding the influence of potential volumetric changes in cerebrospinal fluid (CSF) (Figure 3.1 B). The background was selected with a slice-by-slice mask relative to the peak frequency in the pixel intensity histogram. A threshold was then chosen by adding the difference between the average intensity across all scans and the current scan to a common value. MRI slices were cubically up-sampled and contoured in MATLAB (Ver. 2015a, Mathworks, Natick, MA) with the computed threshold (Figure 3.1 C,D). The optic nerve head (ONH) location was manually specified for each case using multiplanar reconstruction (MPR) tool within the OsirixMD DICOM viewer (version 8.0.1, Pixmeo, Geneva, Switzerland). Linear interpolation between contours (600 μm slice spacing) was applied to obtain a single contour located 3 mm posterior to the ONH along the nerve trajectory. Contours at varying distances from the ONH also could be generated providing a 3D representation of the ON and ONS (Figure 3.1 E). Both cross-sectional areas 3 mm posterior to the ONH were then computed to provide congruency for comparison with results found in other modern ophthalmic literature [14].

ON Deviation

To quantify changes in ON tortuosity due to HDT, the following methods were applied to generate an ON deviation parameter. The parameter describes the maximum orthogonal distance between the curved ON centerline trajectory and a straight line connecting the ONH and a point on the ON trajectory 20 mm posterior to the ONH. High resolution T1-weighted

sagittal images were collected with 900 µm slice thickness and spacing and 488 µm isotropic pixel size (FOV 250 x 250). Additional sequence parameters included a 9° flip-angle, 1900 ms repetition time, and 2.32 ms echo time. 3D MPR, a feature accessible in Osirix MD dicom viewer (version 8.0.1, Pixmeo, Geneva, Switzerland), was used to manually generate curved ON trajectories. Nerve centerline locations were selected with ~ 1-2 mm spacing and exported as lists of comma-separated (X, Y, Z)-coordinates. An up-sampled spline curve was fit to the points and truncated at a centerline trajectory length of 20 mm posterior to the ONH using MATLAB. A trajectory length of 20 mm was used because this length covered the region of ON kinking previously reported to be present in astronauts[14].

Frankfurt Plane and Gaze Angles

Volunteer subjects were instructed to fixate on a point central to their visual field in the MR scanner in order to both maintain a consistent direction of gaze and reduce motion artifacts. To mitigate inconsistencies in gaze between supine and HDT, lateral and vertical gaze angles were quantified to determine if changes in ophthalmic structures were attributed to changes in gaze. To quantify gaze angle, a reference plane known as the Frankfort horizontal plane (FHP) was identified (Figure 3.2 A). The points defining this plane include both left and right porions (superior point of the external acoustic meatus) and the left orbitale (inferior surface of the orbital crest of the zygomatic bone). All three boney locations (X, Y, Z) were collected for each subject by manual inspection in MPR in Osirix MD. A previous intra- and inter-subject reliability study utilizing T1-weighted images viewed using MPR found excellent

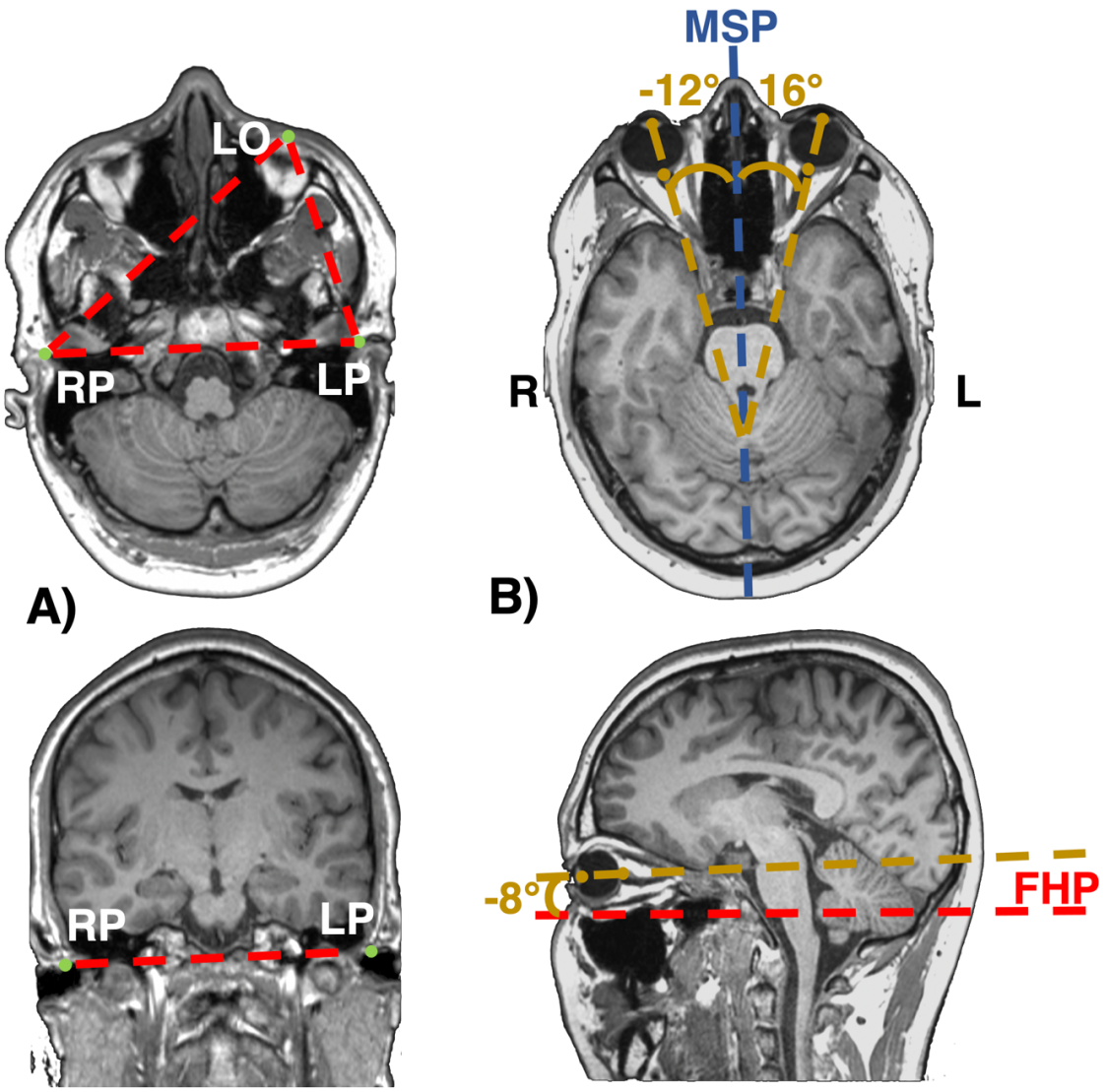

Figure 3.2. Lateral and vertical gaze angles were measured with respect to Frankfurt horizontal plane of the skull. A) High resolution T1-weighted sagittal scan oriented to horizontal and coronal planes to show left and right porion and left orbitale point selections and the resulting Frankfurt horizontal plane (FHP) in red. B) Lateral and vertical gaze vectors measured against the FHP and midsagittal planes (MP).

consistency in defining these landmarks[26]. A midsagittal plane (MP) normal to the FHP was defined by calculating the cross product between the two vectors that can be created from the three Frankfurt points, and was located halfway between the two selected porion points. A gaze vector was defined for each eye as a vector beginning at the ONH and passing through the lens center. These points were previously used to quantify ON deviation and vitreous

chamber depth. Gaze vectors were projected on the FHPs to quantify lateral gaze angles and on the MPs to quantify vertical gaze angels (Figure 3.2 B). Positive and negative lateral gaze values were defined as projections directed in the left and right anatomical field of view, respectively. Positive and negative vertical gaze values were similarly defined as projections directed in the field of view superior and inferior to the FHP, respectively.

Vitreous Chamber Depth

Vitreous chamber depth was used to detect potential posterior globe flattening in HDT subjects and was defined as the distance between manually selected lens and ONH locations. This distance was calculated for both supine and HDT postures in MATLAB by using the comma-separated (X, Y, Z)-coordinates previously defined to assess ON deviation.

ONS Young's modulus Calculation

ONS Young's modulus (E) was estimated utilizing a thick-walled cylinder assumption of the law of Laplace: $E = 3{r_i}^2 r_o \left(\frac{\Delta P}{2\Delta r_o}\right) / ({r_o}^2 - {r_i}^2)$. This calculation requires values for inner (r_i) and outer radius (r_o) of the ONS, and pressure change (ΔP) at the optic axial plane (OAP). The inner radii were calculated for each subject using our MR image-based contouring methods described previously. Dura thickness (t) was specified as 0.4 mm[27]; thus, the outer radii were defined as $r_i + 0.4$. Δr_o was defined as the change in ONS radius derived from the change in ONS area. The hydrostatic equation: $\Delta P = \rho_{CSF} g \Delta h$ was used to estimate pressure change at the OAP, and was calculated utilizing the hydrostatic indifference level (HIL), which was specified as a location between thoracic vertebrae 1 and 2[28]. The change in height (Δh) with

respect to the HIL was approximated as $\Delta h = \sqrt{{d_{OAP}}^2 + {d_{ONH}}^2}[\sin(\tan^{-1}(d_{ONH}/d_{OAP})) - \sin(\tan^{-1}(d_{ONH}/d_{OAP}) - \alpha_t)]$, where α_t is the tilt angle, d_{OAP} is the distance from the HIL to the OAP, and d_{ONH} is the orthogonal distance between the d_{OAP} vector and the ONH [11]. The MRIs collected only included the cranium of each subject causing us to assume a proportional relationship between subject height and the d_{OAP}. We measured the d_{OAP} in a healthy subject from another MRI set with known subject height, and scaled accordingly to obtain an estimated, subject-specific value for d_{OAP}. It should be noted that the effects of the arachnoid trabecula within the subarachnoid space were not considered when estimating Young's modulus of the ONS [29].

Statistics

A linear mixed-effects model that assumed random selection from a population was developed:

$$y_i = \beta_0 + \beta_1 x_{1i} + \beta_2 x_{2i} + \beta_3 x_{3i} + \beta_4 x_{4i} + \beta_5 x_{5i} + z_{0i} + z_{1i} x_{2i} + \epsilon_i$$

Where y_i is the parameter of interest, x_{1i} is treatment group (supine / HDT), x_{2i} denotes which eye (left / right), x_{3i}, x_{4i}, and x_{5i} are the age, body mass index (BMI), and sex of the *i*th subject, respectively. While β represents fixed effect sizes, z represents the random effects, which follows a multivariate normal distribution with mean of 0 and a symmetric variance-covariance matrix:

$$\begin{pmatrix} z_{0i} \\ z_{1i} \end{pmatrix} \sim N\left(\begin{pmatrix} 0 \\ 0 \end{pmatrix}, \begin{pmatrix} \sigma_0^2 & \sigma_{01} \\ \sigma_{01} & \sigma_1^2 \end{pmatrix} \right).$$

The "*fitlme*" function in Matlab (Ver. R2019a Mathworks Corp., Natick, MA) was used to estimate the parameters in this linear mixed-effects model and test the hypothesis. This model appoints treatment group, eye, age, BMI, and sex as fixed effects, with the corresponding coefficient indicating the effect size. We could further test whether the true effect size is significantly different from zero. If so, it means that there is a statistically significant impact on the parameter from treatment groups, eyes, age, BMIs, or sex. This model treats the subjects as random with repeated measurements (on the left and right eye), which allows us to account for the variability across subjects and dependence between the two eyes for each subject.

Using this linear mixed-effects model, we calculated p-values for the following 6 parameters: ON area, ONS area, ON deviation, lateral gaze angle, vertical gaze angle, and vitreous chamber depth. Some of these p-values were dependent due to dependence among several parameters of interest. We accounted for multiple comparison with Bonferroni correction, and adjusted the threshold for p values to be α/m, where α is the experimentwise type I error rate and m is the number of p values under consideration. With six parameters and five fixed-effect sizes per parameter, we have $m = 30$. We consider $\alpha = 0.05$ and $\alpha = 0.10$, with the former being highly conservative and the latter less so.

Results

MR images were collected at supine and 15° HDT for 18 volunteer subjects with average height, weight, and age as 1.63 ± 0.37 m, 67.5 ± 18.3 kg, and 29 ± 12 years, respectively. A summary of all parameter results can be found in Table 3.1. Subjects were occasionally omitted due to MR image artifacts.

Table 3.1. Parameters were developed and quantified to assess changes occurring to ophthalmic structures under HDT. The first column shows the parameter of interest, the second shows the mean change and standard deviation, the third shows statistical significance and the fourth shows the number of subjects and eyes assessed.

Parameter	Mean Change ± SE	p-value	N, eyes
ON Cross-sectional Area (mm^2)	0.15 ± 0.14	0.271	17, 33
ONS Cross-sectional Area (mm^2)	4.05 ± 0.58	0.000	17, 33
ON Deviation (mm)	0.20 ± 0.06	0.002	16, 32
Lateral Gaze Angle (degrees)	0.89 ± 0.64	0.169	16, 32
Vertical Gaze Angle (degrees)	0.10 ± 0.97	0.921	16, 32
Vitreous Chamber Depth (mm)	-0.12 ± 0.04	0.009	16, 32

ON and ONS Cross-sectional Areas

Cross-sectional areas of the ON and ONS were assessed in 17 of the 18 subjects (N = 33 eyes). The average change and standard deviation for ON and ONS areas under HDT were 0.15 ± 0.81 (p = 0.271) and 4.10 ± 3.24 mm^2 (p <0.001), respectively. ON areas that were initially smaller at supine tended to show subtle increases after HDT while larger ON areas in supine appear to decrease in size after HDT (Figure 3.3 C). There is a moderate correlation (R^2 = 0.64) in ON area between supine and HDT (Figure 3.4 A). A clear increase in ONS area was observed during HDT for the majority of subjects excluding a few minimal change cases (Figure 3.3 D). There is strong correlation (R^2 = 0.81) in ONS area between supine and HDT. Bland Altman plots for both ON and ONS areas (Figures 3.4 C, D) show on average increases were observed in both structures with 2 and 1 outliers for ON and ONS, respectively.

ON Deviation

ON deviation was successfully assessed in 16 of the 18 subjects (N = 32 eyes). ON deviation increased by an average of 0.24 ± 0.38 mm ($p < 0.05$) (Figure 3.3 A). A strong correlation ($R^2 = 0.86$) between supine and HDT was observed (Figure 3.5 A). A Bland-Altman plot for ON deviation (Figures 3.5 C) shows an average increase in ON deviation with one outlier.

Gaze Angle

Vertical and lateral gaze angles where successfully quantified in 16 subjects (Figure 3.2 B). Lateral and vertical gaze angles increased by an average of 0.91 ± 3.92 and 0.23 ± 6.61, respectively; however, changes in lateral and vertical gaze angles were statistically insignificant ($p = 0.169$ and $p = 0.921$, respectively). Statistically significant differences in lateral gaze angle between the left and right eyes ($p < 0.001$) were present as a result of subjects focusing at a medial point in their field of view.

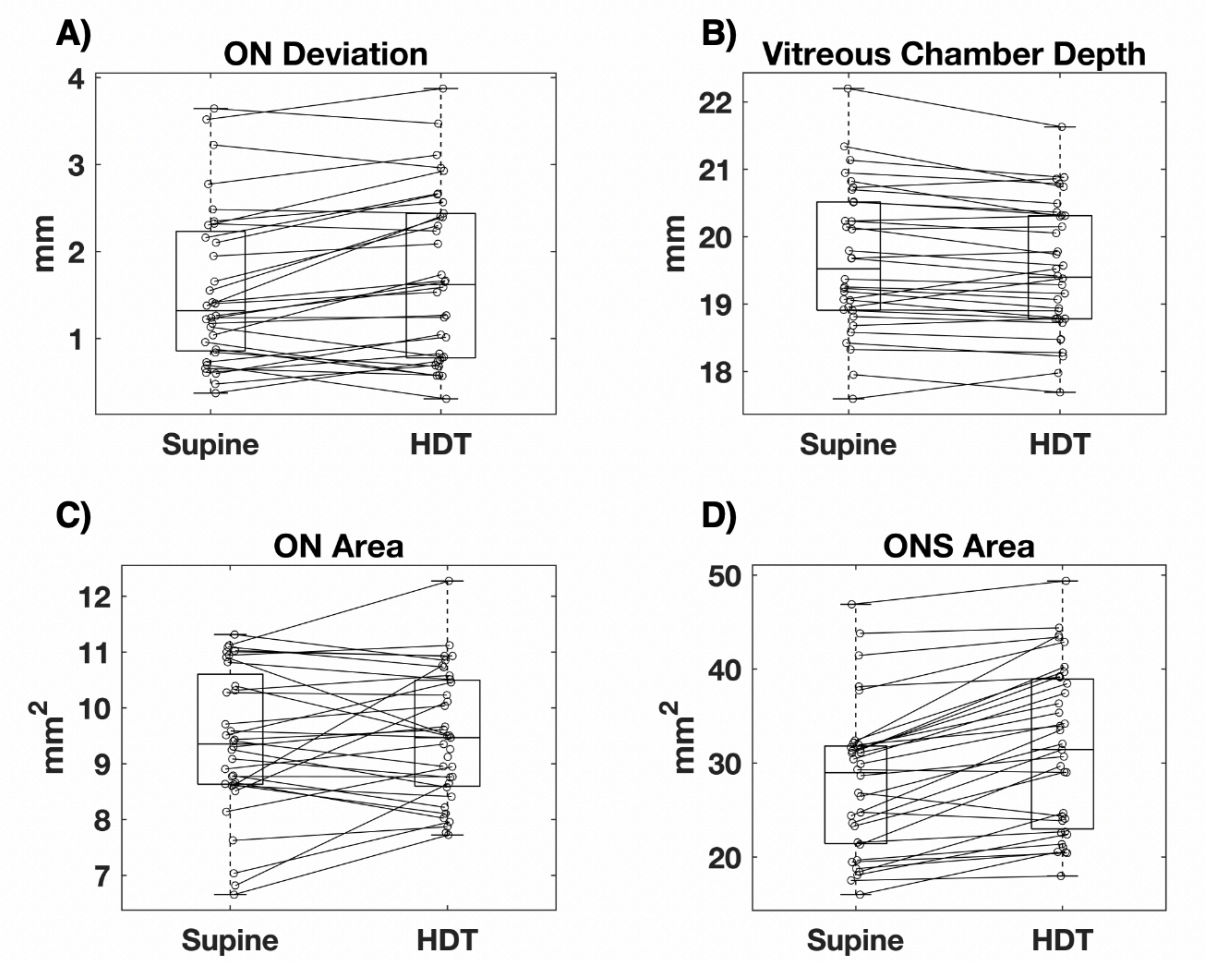

Figure 3.3. Supine and HDT Boxplots of A) ON deviation, B) vitreous chamber depth, C) ON area, and D) ONS area showing how parameters of individual eyes changed from supine to HDT posture.

Vitreous Chamber Depth

Vitreous chamber depth was measured in 16 subjects and showed an average decrease of -0.10 ± 0.25 mm ($p < 0.01$) during HDT (Figure 3.4 B). There was a strong correlation between supine and HDT measurements ($R^2 = 0.95$) and subjects with the longest supine vitreous chamber depths had the largest decreases under HDT (Figure 3.5 B). A Bland Altman plot for vitreous chamber depth (Figure 3.5 D) shows that there are two outliers.

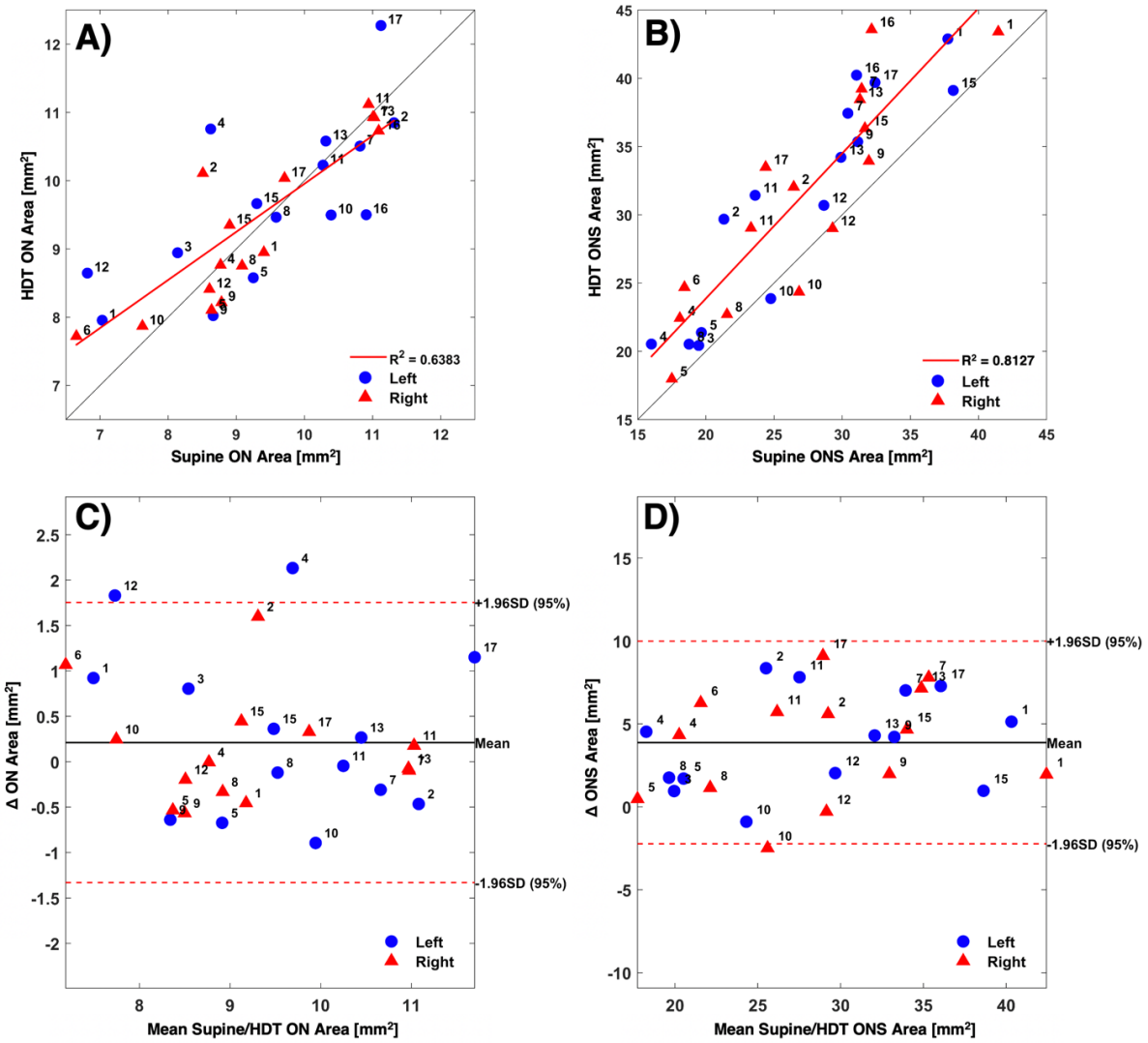

Figure 3.4. Concordance correlation of A) ON and B) ONS cross sectional area at 3mm posterior to the ONH under supine and HDT conditions. Linear regression between both timepoints is shown in red. Bland-Altman plots of C) ON and D) ONS cross sectional area. Blue circles and red triangles represent left and right eyes, respectively. Subject numbers are displayed next to their respective data points.

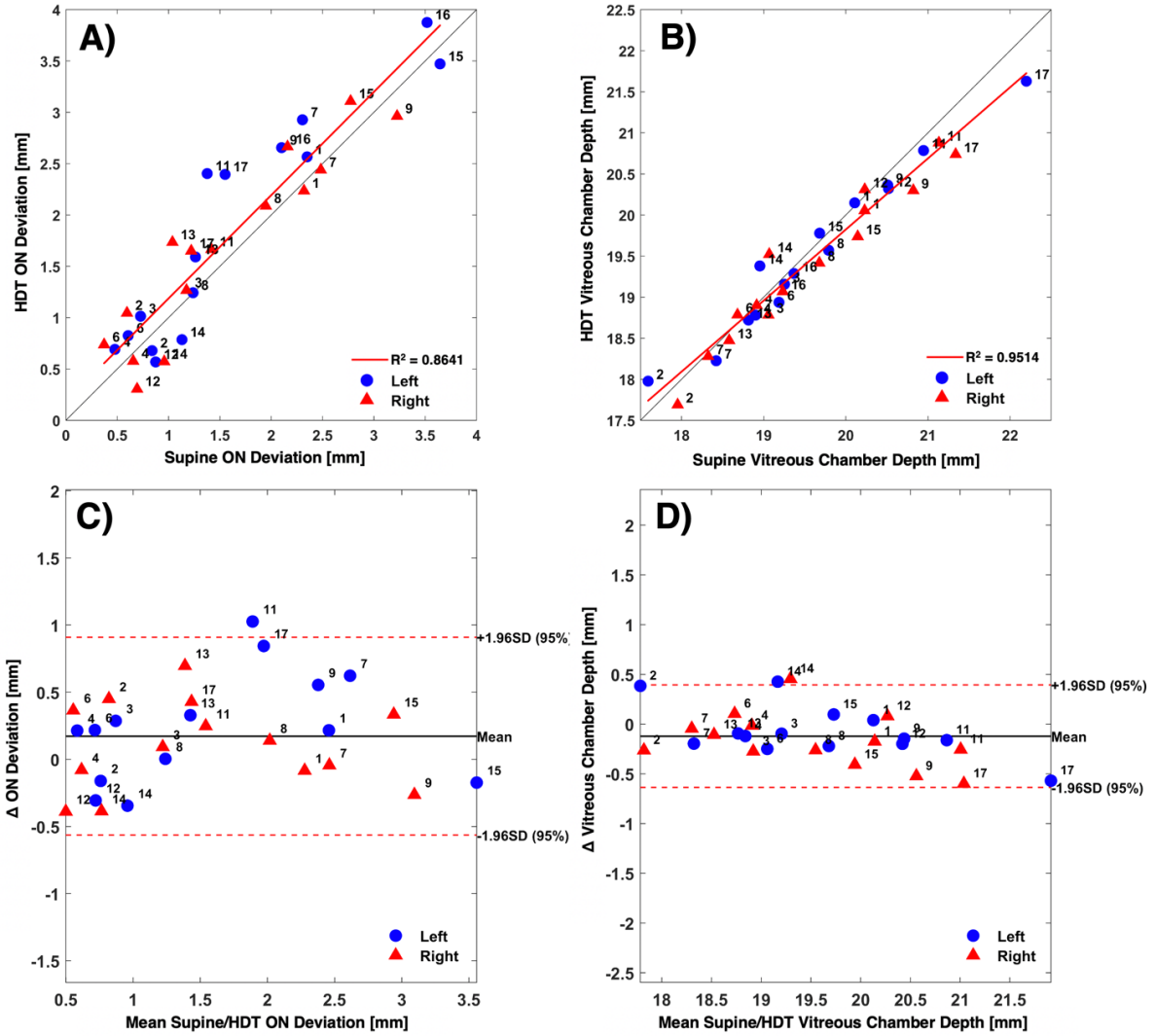

Figure 3.5. Concordance correlation of A) ON deviation and B) vitreous chamber depth under supine and HDT conditions. Linear regression between both timepoints is shown in red. Bland-Altman plots of C) ON deviation and D) vitreous chamber depth. Blue circles and red triangles represent left and right eyes, respectively. Subject numbers are displayed next to their respective data points.

Demographic Effects and Unilaterality

All parameters were assessed for covariates including BMI, age, sex, and eye to determine if any of the observed changes could be partially attributed to demographic differences or unilaterality. BMI accounted for a decrease of 0.14 mm^2 in ON area ($p < 0.05$) and a decrease of 0.15 mm in ON deviation ($p < 0.005$). Females had a decrease of 10.98 mm^2

in ONS area ($p < 0.005$) when compared to males. All other covariates were insignificant including differences between the left and right eyes.

ONS Young's modulus

ONS Young's modulus 3 mm posterior to the optic head was estimated for 16 subjects. Subjects were omitted when ONS area was unchanged or decreased during HDT. The mean and standard deviation of ONS Young's modulus was 85.0 ± 115.7 kPa.

Discussion

Non-invasive automated and manual techniques were developed and applied to MR images to quantify changes in ophthalmic structures during acute HDT and estimate Young's modulus of the ONS. The ONS cross-sectional area was found to increase under HDT while the ON cross-sectional area remained unchanged. ON deviation was also found to increase, an indication of increased tortuosity. While changes in lateral and vertical gaze angles were observed, no significant trends were identified between supine and HDT. A decrease in vitreous chamber depth suggests that HDT may contribute to alterations in the geometry of the optic globe. A thick-walled cylinder assumption of the law of Laplace was applied to estimate an ONS Young's modulus of 85.0 kPa. The findings reported here can be compared to structural changes observed in astronauts to better understand the role of CSF redistribution in the development of SANS.

The ONS is known to be sensitive to changes in ICP due to communication between the orbital subarachnoid space surrounding the optic nerve and cranial subarachnoid space [30]. Thus, the ONS distension observed within the bulbar subarachnoid region suggests that CSF

pressure was pathologically elevated during acute 15° HDT. The magnitude of the distension in the majority of subjects shows a propensity of the ONS to compensate for elevated ICP. However, there is a presumable pressure where the compensatory threshold of the ONS becomes saturated, and further increases in ICP would result in insignificant changes in ONS area[31]. Subjects who had little to no change in ONS area may have had elevated ICP when in the supine position and had already reached the compensatory threshold. The lack of changes in the ON area suggest that the ON is resistant to intra- and extravasation of CSF during pressure fluctuations.

ONS Young's modulus has been estimated using a variety of methods but almost exclusively ex vivo. Lee et al. used finite element modeling to estimate the in vivo stiffness of the ONS in the same subjects reported here, and found a mean Young's modulus of 47 kPa[11]. This is similar to the Young's modulus we calculated in the subarachnoid region of the ONS. However, ex vivo measurements of porcine ONS stiffness reported by Wang et al. are orders of magnitude greater (8.57 MPa vs 0.085 MPa)[32]. This difference is likely attributed to their use of uniaxial tensile testing in the axial direction that ignores the anisotropic nature of ONS tissue. The ONS is thought to be much more resistant to axial deformation than the circumferential deformation that was measured in this study[33]. It should be noted that the effects of the arachnoid trabecula within the subarachnoid space were not considered when estimating Young's modulus of the ONS[29].

Tortuosity and kinking of the ON has been observed in astronauts after long-duration spaceflight through the subjective analysis of postflight MR images[14]. However, this study lacked baseline MR images that permit thorough comparisons. More recent studies that

include baseline comparisons failed to identify significant changes in ON tortuosity[34] or ON deviation[7] after spaceflight. In contrast, the present study identified significant increases in ON deviation during HDT exposure, which may impose abnormal mechanical stresses on the ON and ONS. To our knowledge, this is the only study to quantify ON deviation in HDT subjects.

A linear mixed-effects model was used to account for the potential impact of demographics and eye unilaterality on the observed structural changes. Age was not found to be contributing factor to any of the observed changes; however, the range of ages in this study was small. Females showed much greater change in ONS area and vitreous chamber depth when compared to males, suggesting females may be more susceptible to the effects of CSF redistribution. While BMI was higher in males than females in this study, it was only associated with changes in ON area and ON deviation and was not associated with changes in ONS area.

HDT studies have been used to simulate the fluid redistribution experienced in microgravity[35]. One such study invasively measured ICP in rhesus monkeys under 6° HDT and found that ICP was almost immediately elevated but then slowly reduced over the course of 15 minutes[36]. The 30-minute HDT duration in the present study may have been sufficient to result in significant reduction in ICP before scans were taken, although the observed ONS distension suggests ICP was still elevated well beyond supine levels. In a study by Marshall-Goebel et al., healthy subjects were placed in 3 different HDT positions (6°, 12°, and 18°) for 3.5 hours after which ICP and IOP was non-invasively measured. ICP was found to increase significantly during 18° HDT ($p < 0.001$), while IOP increased significantly during 12° ($p < 0.001$) and 18° ($p < 0.001$) HDT[25]. The increase in IOP indicates a propensity for IOP to counteract globe flattening at lower HDT angles. However, reduced vitreous chamber depth identified in

our study suggests that IOP is not sufficiently elevated during 15° HDT to maintain a nominal trans-laminar pressure gradient with ICP.

While HDT conditions have shown to simulate headward fluid redistribution experienced in microgravity, the magnitude of redistribution under HDT may be greater. The peripapillary total retinal thickness identified in healthy subjects after 30 days of strict 6° HDT increased to a greater degree than astronauts after a similar flight duration[21]. Furthermore, ONS distension was not identified after long-duration spaceflight when the methods used here were applied to astronauts[7]. The significant ONS distension we identified in HDT subjects supports the notion that HDT could result in a higher ICP than what would be expected in microgravity.

The methods reported here involve several limitations. Manual selection of the ONH as a reference point for the purpose of locating the ON position 3 mm posterior to the ONH inherently introduces error. Similar error may be introduced in manual selection of the lens center and ON centerline path. However, we considered this error to be acceptable based on an inter and intra-operator reliability assessment of these methods performed by Rohr et al.[7]. Accuracy and resolution of the methods used have yet not been defined. A longitudinal comparison with a healthy control subject is necessary to test the repeatability of the method. Weaker correlation between the supine and HDT ON measurements compared to the ONS measurements suggest that the automated method is not as sensitive to detecting changes in the ON area.

Quantitative MRI-based assessment of the ON and ONS before and during HDT could help our understanding of SANS and the potential role of ICP in the physiological response of

ophthalmic structures. Here we report no change in ON area, but significant increases in ON deviation and ONS area were identified as a result of HDT. These findings suggest that CSF pressure within the bulbar subarachnoid space was pathologically elevated during acute 15° HDT. Further research is warranted to quantitatively assess ON parameters in varying HDT durations and angles.

Chapter 4: Automated MRI Based Quantification of Posterior Globe Deformation Recovery After Long-duration Spaceflight

Forthcoming in Nature - Eye

Abstract

Spaceflight associated neuro-ocular syndrome (SANS), a human health risk related to long-duration spaceflight missions, is hypothesized to result from a headward fluid shift that occurs with the loss of hydrostatic pressure gradients in weightlessness. Fluid shifts in the vascular and cerebrospinal fluid compartments may alter the mechanical forces at the posterior eye and lead to tissue deformation, such as flattening of the posterior ocular globe. The goal of the present study was to develop and apply an automated method to quantify posterior globe flattening observed by magnetic resonance imaging (MRI) after long-duration spaceflight.

Volumetric displacement of the posterior globe was quantified in 10 astronauts (mean ± standard deviation, age 42.9 ± 5.6 years) at 5 time points after spaceflight missions of ~6-months. Mean globe volumetric displacement was 9.88 mm^3 (95% CI 4.56 to 15.19 mm^3, $p < 0.001$) on the first day of assessment after the mission (R (return)+ 1 day); 9.00 mm^3 (95% CI 3.73 to 14.27 mm^3, $p = 0.001$) at R+30 days; 6.53 mm^3 (95% CI 1.24 to 11.83 mm^3, $p < 0.05$) at R+90 days; 4.45 mm^3 (95% CI -0.96 to 9.86 mm^3, $p = 0.12$) at R+180 days; and 7.21 mm^3 (95% CI 1.82 to 12.60 mm^3, $p < 0.01$) at R+360 days.

There was a consistent inward displacement of the posterior globe at the optic nerve in most subjects, which had only partially resolved 1 year after landing. More pronounced globe flattening has been observed in previous studies of astronauts; however, those

observations lacked quantitative measures and were subjective in nature. The novel automated MRI-based method described here allows for detailed quantification of structural changes in the posterior globe that may lead to an improved understanding of SANS.

Introduction

More than half of the astronauts who participate in long-duration spaceflight missions present with neuro-ocular changes that can affect visual acuity. These changes can include choroidal folds, optic disc edema, hyperopic shifts, and posterior globe flattening, and these symptoms are associated with spaceflight associated neuro-ocular syndrome (SANS)[2,14,19,20]. The severity of visual disturbance reported by astronauts appears to increase with the duration of spaceflight, and some of these disturbances are unresolved after return to Earth[21,22]. Globe flattening occurs when the convexity of the posterior aspect of the sclera is reduced and the axial length of the globe decreases, which drives a hyperopic shift in refractive error.

Mader et al. described a case study of one astronaut with globe flattening associated with spaceflight[19]. In addition, Kramer et al. observed globe flattening in 7 subjects in a cohort of 27 astronauts[14]. However, in both of these studies, globe flattening was determined subjectively and retrospectively, with limited preflight baseline scans available for comparison. Here we report the first prospective quantitative analysis of spaceflight-induced globe flattening from magnetic resonance imaging (MRI).

A leading hypothesis for the underlying pathophysiology of SANS, including globe flattening, is a sustained cephalad fluid shift during long-duration exposure to microgravity[37]. Because the intracranial and postorbital cerebrospinal fluid (CSF) space communicate,

changes in intracranial pressure (ICP) may cause a reversal of the translaminar pressure difference (TLPD) at the posterior eye, i.e. ICP can become greater than intraocular pressure (IOP). Such a reversal could cause the sclera to become flattened, as seen in patients with idiopathic intracranial hypertension (IIH)[38-41].

The aim of this study was to quantify spaceflight-induced volume displacement of the posterior ocular globe and to assess the recovery profile for 1 year after flight in an astronaut cohort. To accomplish this, we developed an automated method to perform segmentation of the ocular globe from MR images. The resulting segmentations were parameterized to compare posterior globe shape to preflight (baseline) shape.

Methods

Study Participants

This study included 10 astronauts who participated in missions on the International Space Station (n = 20 eyes, mean ± standard deviation (SD) age: 42.9 ± 5.6 years, body mass index: 24.0 ± 1.8 kg/m^2, and flight duration: 167 ± 17 days). Astronauts were scanned 508 ± 230 days before flight, as well as at 4 ± 2 days (R+1), 31 ± 5 days (R+30), 101 ± 14 days (R+90), 196 ± 34 days (R+180), and 359 ± 19 days (R+360 days) postflight, allowing for a longitudinal analysis of postflight recovery. Data from 22 timepoints that were collected from 8 different subjects were excluded from the analysis due to gradient artifacts, errors caused by movements, or because the intensity of the MRI was inhomogeneous. The MRI data collection protocol for this study was approved by the NASA and University of Idaho institutional review boards and satisfied all local and international regulations for human subject research. All

subjects provided informed written consent before participating in the study. Data was de-identified before being transferred to the University of Idaho for analysis.

MRI Acquisition and Reformatting

T2-weighted axial spin-echo fat-suppressed MRI sequences were collected using a 3T system (Verio 3T; vB19; Siemens Healthineers, Erlangen, Germany) with 0.39 mm in plane isotropic pixel size (FOV 100 x 100), and 0.80 mm slice thickness and spacing. Additional sequence parameters included a 170° flip angle, 750 ms repetition time, 111 ms echo time, and 211 Hz/pixel bandwidth.

MRI scans of each orbit were radially resliced in Osirix (version 8.0.1, Pixmeo, Geneva, Switzerland) at 1-degree increments (180 slices) about a central rotational axis (Figure 4.1 A). This ensured consistent slice orientation orthogonal to the scleral surface. The rotation axis was defined by manual selection of the optic nerve head (ONH) centroid and lens center, through which a view axis was aligned. The ipsilateral lens and ONH points were triangulated with the contralateral ONH point to manually define an axial plane. Each slice was exported as a 16-bit image with 512 rows and columns with minimal padding around the globe.

Generation of Point Cloud

Three dimensional reconstructions of each globe were created and mapped to a common coordinate system using a multistep process in MATLAB (vers 2019a, Mathworks Corp. Natick, MA.). Global thresholding was used to segment the posterior globe (Figure 4.1 B). To account for variations in scan intensity, a histogram-based selection of background

pixels was used to compute a threshold offset[7]. Each slice was cubically up-sampled by a factor of four before applying a threshold value of 380 plus the predetermined offset for the respective scan. The initial threshold of 380 was chosen based on anatomical inspection of the resulting geometries with respect to the scleral margin and maximization of the total number of analyzed subjects. Previous MRI imaging studies have identified the sclera to be the markedly hypointense region on T2 images, with the retina and choroid presenting as a multilayered structure [42-44]. Based on comparison with these studies, our segmentation scheme identified a boundary near the exterior margin of the retinal/choroidal structure, i.e. slightly interior to the scleral/choroidal margin (Figure 4.1 C). We consider this boundary to be a reasonable representation of the inner surface of the ocular globe (see Discussion), and will thus refer to our segmentation procedure as “globe segmentation” going forward.

After thresholding, a flood fill operation was applied to preserve only the inner region of the globe. Next, the edge points of the globe were collected and transformed to 3D MRI coordinates. Every point cloud was downsampled using a box grid filter (MATLAB, computer vision toolbox, pcdownsample) with a filter size of 0.5 to ensure that the points were uniformly spaced (Figure 4.1 D). The downsampled point clouds were then used in an alignment process. This process involved choosing a preflight point cloud as a baseline and registering each subsequent postflight point cloud using an iterative closest point algorithm (MATLAB, computer vision toolbox, pcregistericp) with 60 iterations (Figure 4.1 E).

Generation of Displacement Map

Displacement maps were generated to visualize changes in the posterior globe. First, the centroid for each eye was defined by averaging the locations of all points in the downsampled preflight point cloud. Next, a set of coordinate axes was created from the normal vector to the manually defined axial slice and the axis joining the ONH to the centroid. Using these two vectors, a circumferential and meridional coordinate system was created as described by Grytz et al.[45]. The spherical coordinates of each point on the globe surface was then expressed in polar coordinates, i.e. circumferential and meridional angles were transformed into a polar angle and radial location, and radius was represented by a color on the pre- and postflight distance maps. These points were interpolated onto a square grid to allow for pairwise comparison between the distance maps (Figure 4.1 F).

For each point on the ocular surface, a vector was defined from the centroid to that point, and the vector's magnitude (length) was represented by a color ranging from red to blue (Figure 4.1 F). A (postflight - preflight) displacement map of the posterior globe was created by subtracting these vector magnitudes (Figure 4.1 F), and displacements for surface points lying within a 4 mm radius of the ONH were quantified. A mean globe displacement value was computed based on the average displacement within this 4 mm radius. The associated volumetric change was determined by calculating the volume of a cylinder with a height equal to the mean displacement and a radius of 4 mm.

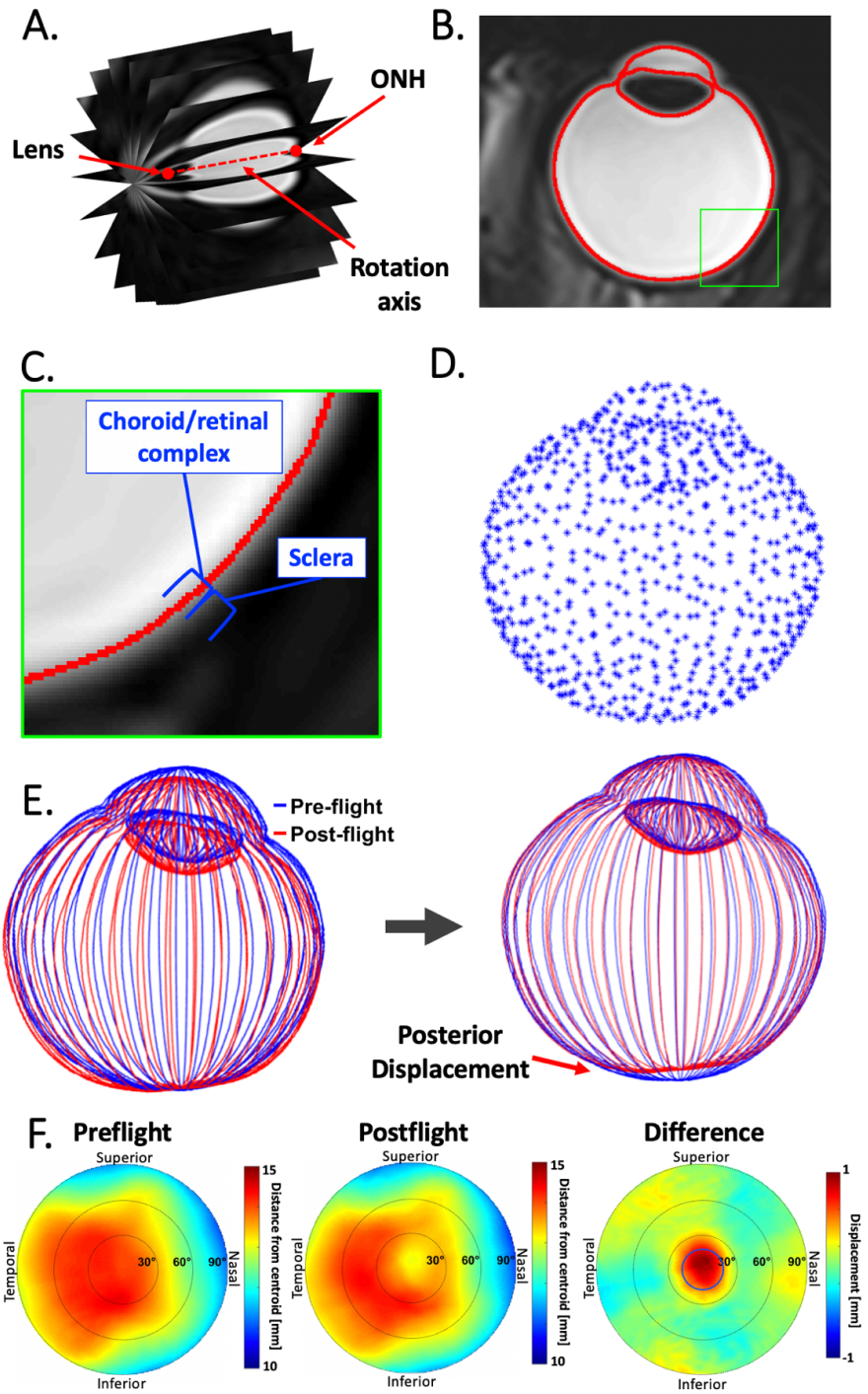

Figure 4.1. Methods for segmenting T2-weighted axial ocular MRI. (A) MR images were radially re-sliced, and (B) automatically segmented. (C) Zoomed in view of the posterior globe (green square on panel B), showing the sclera (hypointense region), the putative retinal/choroidal complex, and the boundary identified by our segmentation scheme (red curve). (D) shows 3D reconstructed down sampled point cloud, and (E) demonstrates the registration of point clouds. (F) Example pre- and postflight distance maps and the resulting differential displacement map for the posterior surface of one eye with notable globe flattening, with the 4mm region of interest (blue circle) around the optic nerve head on the displacement map. Note: the indicated tissue regions in panel (C) are approximate since it is impossible to precisely demarcate the scleral and retinal/choroidal boundaries.

Ocular Measures

Axial lengths have been previously reported by Macias et al.[22] and are presented here to compare with globe flattening variables. In brief, axial length, i.e. the distance between the anterior surface of the cornea and the fovea, was measured before and after spaceflight using optical biometry (IOLMaster 500; Zeiss). Fundoscopy was performed on all crewmembers after flight as part of the standard postflight medical assessment. Presence of optic disc edema on fundus images was determined using the modified Frisén grading system.

Statistics

Statistical analyses were conducted using Stata/SE (v 16.0), setting 2-tailed alpha to reject the null hypothesis at 0.05, with an emphasis on characterizing the observed effects and reporting statistical significance. Our experimental design was a mixed-factorial, with repeated observations nested within astronaut (left and right eye) and over time (several postflight time points), each representing a delta score from astronauts' preflight values. All our outcomes were continuously scaled and were analyzed using Gaussian-based maximum likelihood mixed-effects modeling that included 2 random Y-intercepts for the nesting of left and right eye measurements within time period and to accommodate for the repeated-measures over time. We included a fixed-effects covariate parameter to adjust for each astronauts' prior exposure to weightlessness (i.e. the number of previous flight days), and a priori contrast to compare delta scores at each time point (relative to preflight score) to zero. Statistical

assumptions were tested before interpreting results, and 1 (out of 77) overly influential observation was eliminated from our evaluation of the novel volume displacement outcome because it had a standardized residual that exceeded ± 2, which skewed overall distribution of residuals. We used Somers' d measure of association and Bland & Altman plots with 95% levels of agreement references to evaluate the strength of association between the changes in ocular displacement and the changes in optical biometry, incorporating the nesting of observations within astronaut.

Results

Nearly all subjects exhibited some degree of globe flattening (Table 4.1). However, the degree of globe flattening was relatively small when compared to the average reported vitreous chamber volume of 4650 and 4969 mm^3 in women and men, respectively[46], with an average volume displacement of 9.88 mm^3 (95% CI 4.56 to 15.19 mm^3, $p < 0.001$) measured at R+1 (Table 4.1 and black line in Figure 4.2 A). During the postflight follow-up scans, mean volume displacement was 9.00 mm^3 (95% CI 3.73 to 14.27 mm^3, $p = 0.001$) at R+30; 6.53 mm^3 (95% CI 1.24 to 11.83 mm^3, $p < 0.05$) at R+90; 4.45 mm^3 (95% CI -0.96 to 9.86 mm^3, $p = 0.12$) at R+180; and 7.21 mm^3 (95% CI 1.82 to 12.60 mm^3, $p < 0.01$) at R+360. Notably, the subject with the greatest volume displacement (22.43 mm^3 in the left eye and 39.16 mm^3 right eye) also presented with Frisén grade 1 optic disc edema (Subject 2, Figure 4.3).

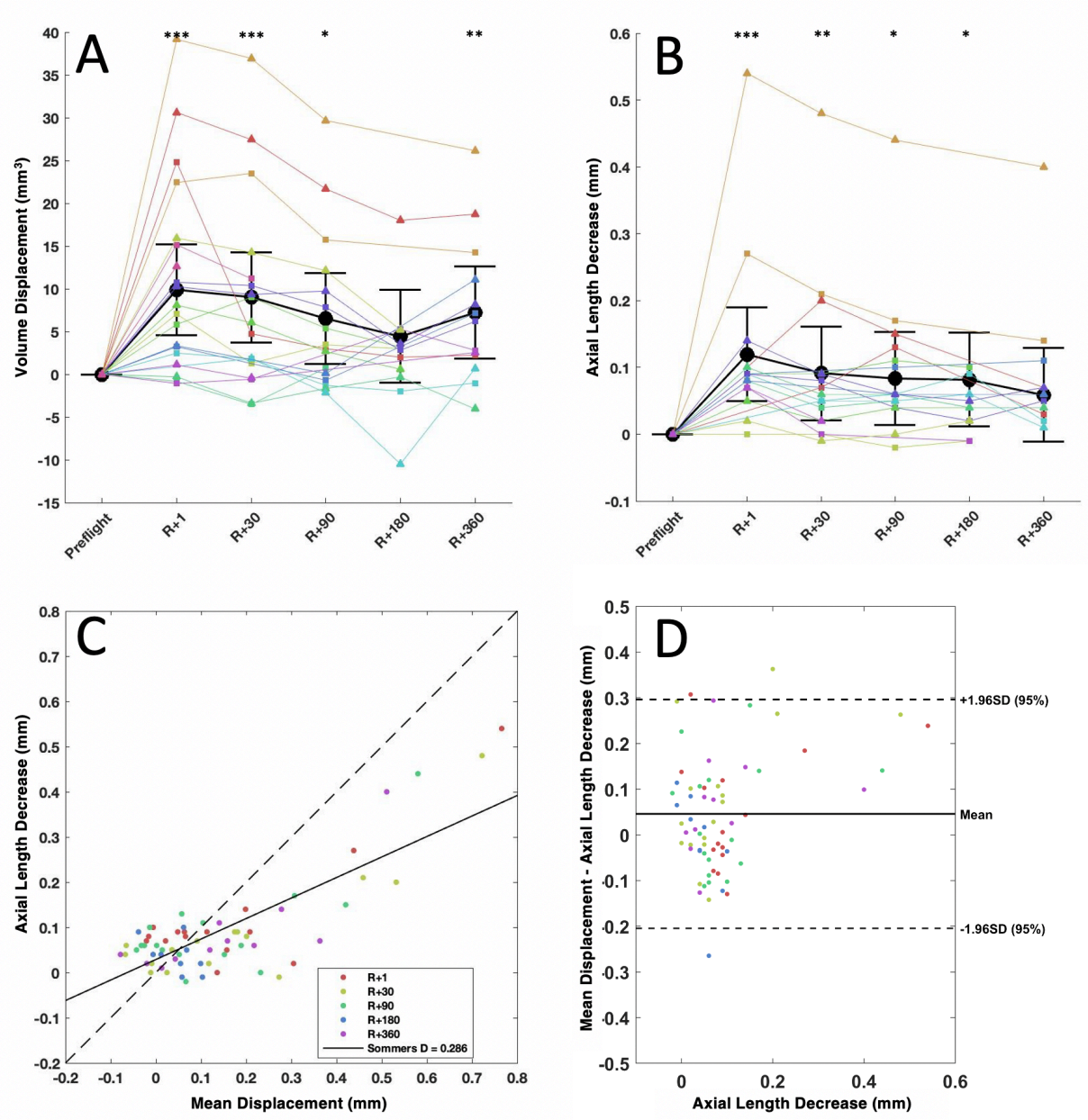

Figure 4.2. Plots showing pre- to postflight (A) MRI-assessed volume changes in the posterior ocular globe and (B) optical biometry-assessed axial length decreases at multiple time points after return to earth (R+; days) postflight. All changes are referenced to preflight values. Triangles and squares represent right and left eyes, respectively. Each subject is shown in a different color, with yellow representing the subject diagnosed with grade 1 optic disc edema. Black markers and error bars represent mean values with 95% confidence intervals and black stars indicate statistical significance from preflight baseline. Volume displacement within a 4 mm radius of the optic nerve head was averaged and compared with ocular axial length decreases (pre-post) as measured by ocular biometry using (C) correlation and (D) Bland-Altman plots. Note: panel B was created using data adapted from Macias et al. [47]. *p<0.05, **p<0.01, ***p<0.001

The average decrease in axial length acquired by ocular biometry at R+1 was 0.12 mm (95% CI 0.19 to 0.05 mm, p = 0.001), which partially recovered to 0.05 mm (95% CI 0.13 to 0.01 mm, p = 0.09) by R+360 (Table 4.1). Volume displacement from MRI was used to generate the mean displacement parameter that could be compared with ocular biometry measurements. The average values of the mean displacement were 0.20 mm (95% CI 0.09 to 0.30 mm, p < 0.001) at R+1; 0.18 mm (95% CI 0.07 to 0.28 mm, p = 0.001) at R+30; 0.13 mm (95% CI 0.02 to 0.24 mm, p < 0.05) at R+90; 0.09 mm (95% CI –0.02 to 0.20 mm, p = 0.12) at R+180; and 0.14 mm (95% CI 0.04 to 0.25 mm, p < 0.01) at R+360.

The mean difference between decrease in axial length from optical biometry and the mean displacement was 0.05 ± 0.12 mm. Linear correlation yielded an R^2 of 0.62 and Sommers' d of 0.286 (Figure 4.2 C). The Bland-Altman plot (Figure 4.2 D) shows agreement between these variables with most of the data points lying within the 95% confidence range.

Table 4.1. Mean and standard error of MRI-assessed posterior ocular globe changes from preflight (baseline), including change in volume, axial length (assessed by optical biometry), and mean displacement.

Parameter	R+1	R+30	R+90	R+180	R+360
Volume Decrease (mm^3)	9.88 ± 5.31***	9.00 ± 5.27***	6.53 ± 5.29*	4.45 ± 5.41	7.21 ± 5.39**
Δ Ocular Biometry (mm)	-0.12 ± 0.07***	-0.09 ± 0.07**	-0.08 ± 0.07*	-0.08 ± 0.07*	-0.06 ± 0.07
Mean Displacement (mm)	0.20 ± 0.11***	0.18 ± 0.11***	0.13 ± 0.11*	0.09 ± 0.11	0.14 ± 0.10**
Number of Subjects, Eyes	9, 17	9, 18	10, 18	7, 12	7, 13

Key: p<0.05 *, p<0.01 **, p<0.005,***

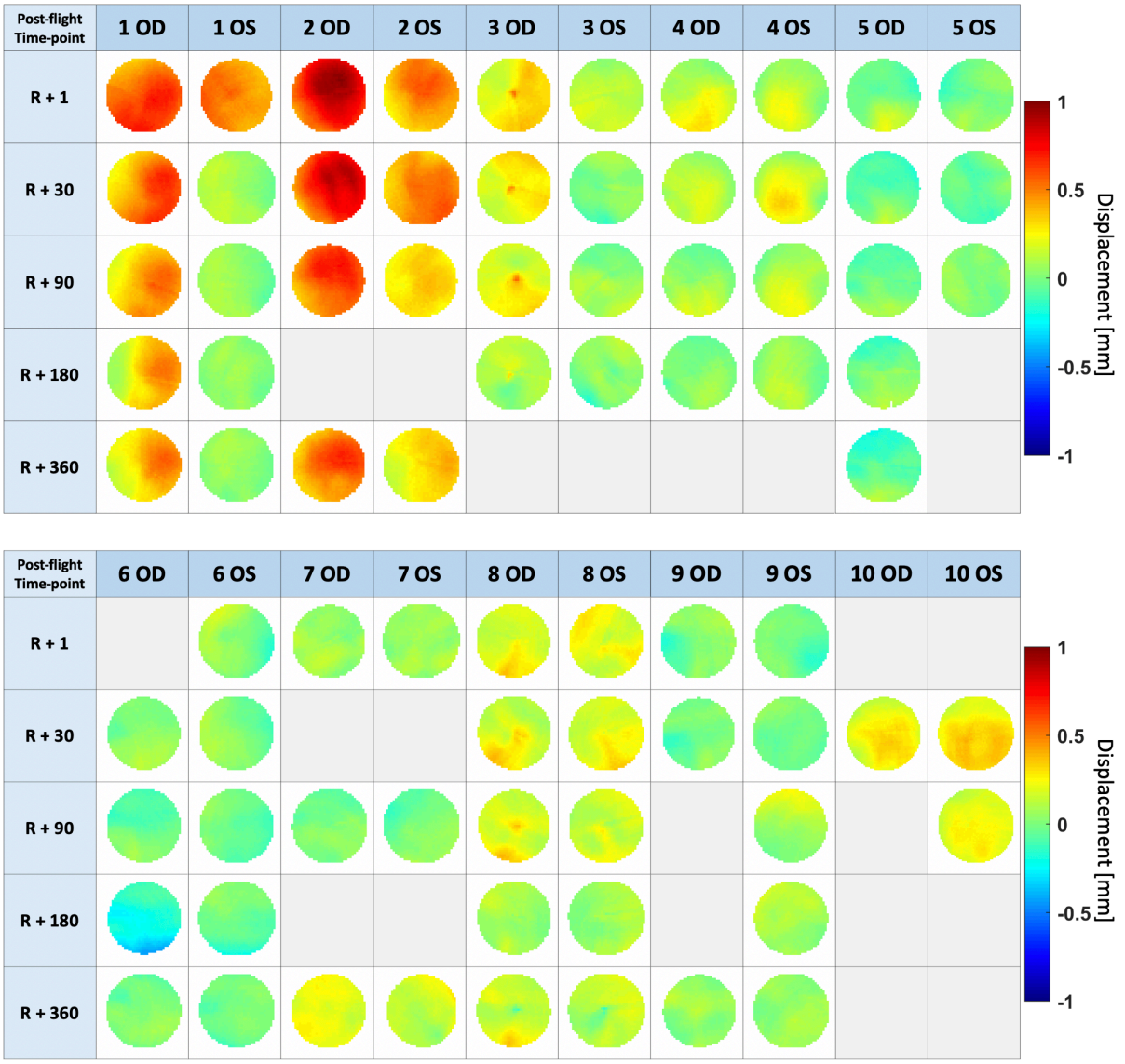

Figure 4.3. Summary of all globe displacement maps for each subject (within a 4 mm radius around the optic nerve head) at multiple time points after postflight recovery (R+1, R+30, R+90, R+180, and R+360 days). OS and OD refer to left and right eye respectively. Grey boxes indicate that data was not available for that time-point. The subject with the most severe displacement (subject 2, OD) was clinically diagnosed with grade 1 optic disc edema via fundus imaging (i.e., SANS).

Discussion

Here we present an objective, MRI-based volumetric quantification of changes in the posterior globe of astronauts after ~6-month spaceflight missions. Our findings provide a quantitative analysis of individual posterior ocular globe volume displacement due to spaceflight, as well as postflight recovery of these changes, and our study lends support to

previous subjective assessments of globe flattening in astronauts[14,19,37,48]. Our findings suggest that pathological globe flattening is not widespread; however, there is a consistent trend of small, inward displacements of the peripapillary choroidal-scleral interface in most subjects after long duration (~6-months) spaceflight. These displacements tended to be unidirectional within the region of interest, i.e. there were no instances where displacements occurred in both directions to create no net change within the 4 mm radius analyzed. The magnitude of inward displacement of the posterior globe decreased over time after return to Earth; however, on average, it had not returned to preflight baseline value by 1-year after spaceflight. Notably, one astronaut in our cohort with Frisén grade 1 optic disc edema also had the greatest degree of posterior globe volume displacement. Our data are consistent with ocular biometry measurements which show that globe axial length did not return to preflight values by R+360 (Figure 4.2 B)[22].

The longitudinal nature of this study and inclusion of multiple postflight recovery timepoints provides a unique quantitative assessment of spaceflight-induced globe flattening and its recovery, showing a clear association between the magnitude of globe volume displacement and duration of time after spaceflight. We speculate that displacement may have been more severe inflight but began recovering before the first postflight scan took place, occurring on average 4 days after return to Earth.

It is important to note that our segmentation methods detect an anatomic boundary near the choroidal/scleral interface, and thus the displacement we compute could be due to morphometric changes other than scleral flattening, i.e. our displacement parameter combines globe flattening with choroidal swelling. However, the average mean displacement

measured in this study far exceeded the average combined increase in total retinal and choroidal thickness identified using optical coherence tomography by Macias et al.[22]. Moreover, spaceflight induced total retinal and choroid thickening on average recover to preflight values by 90 days after landing[47]. Thus, changes in the choroid cannot explain the large displacements that we observed in most subjects, and throughout we use the term "globe flattening" to describe the morphological changes that we have observed.

Several studies have reported clinical ocular examinations of astronauts who participated in long-duration spaceflight. Mader et al. subjectively identified globe flattening and optic disc edema in 5 of the 7 astronauts they assessed, and identified thickening of the retinal nerve fiber layer in 6 of 7 astronauts[19]. In 3 of these 7 astronauts, globe flattening persisted for at least 7 years following spaceflight [4]. A 2017 case report described an astronaut who developed asymmetric optic disc edema during spaceflight, which remained unresolved 630 days after flight [48]. Optic disc edema was also identified in an astronaut cohort similar to the cohort assessed in the present study, and the reported recovery pattern for the optic disc edema was similar to that of the recovery of globe flattening presented here[22]. Subjective, MRI-based clinical reporting by Kramer et al. identified globe flattening in 7 of 27 astronauts[14].

Semi-automated MRI-based mapping of the optic globe has been performed previously in several studies (Table 4.2), with each study producing different parametrizations. These parameterizations require development of a coordinate system that depends on anatomical reference points, typically accomplished by image registration and definition of an anatomical axis. In this work, we used an iterative closest point algorithm with a least squares metric to minimize the differences between matching point clouds. This is considered to be a

conservative approach because all points are weighted equally. Performing registration after segmentation helps align the unanchored globe in MRI images, but could introduce error from segmentation artifacts and loss of volumetric information. The fairness of the registration depends on point cloud uniformity, which was enforced with a box-grid filter. Our segmentation was aided by radially reslicing the MRI scan of the orbit (Figure 4.1 A) to obtain consistent intervoxel averaging of the edge of the globe. This highly automated registration method, in combination with the advanced multi-timepoint study design, adds rigor to the current study. Using a different approach, Jinkins et al. was able to subjectively identify optic nerve head (ONH) protrusion in 10 of 15 patients with elevated ICP using MRI[49]. Alperin et al. applied a mapping technique to measure globe flatness in IIH patients. When compared to a control group, IIH patients showed a globe flatness index increase of 0.02[38], corresponding to a linear displacement of approximately 0.24 mm, similar to the average mean displacement we found in astronauts.

Table 4.2. Comparison of various MRI-based methods used to quantify optic globe structure.

Method	MRI Protocol	Key Finding and Measures	Citation
Segmentation Expectation-maximization **Parameterization** Axial plane matching with rigid linear MRI registration; Orthogonal coordinate system with respect to axis formed by lens center to globe center of mass.	1.5/3T T2 3D CISS: 0.6 mm in plane isotropic; slice thickness, 0.6 mm; TR, 6.35/5.42 ms; TE, 2.82/2.43 ms; flip angle, 47/34°; pixel bandwidth, 560/650 Hz/pixel	Posterior globe is altered in IIH * 2D cartesian deformation map and corresponding measures: nerve protrusion (NP), globe flattening (GF), maximum deformation (MD) * Control, IIH mean ± SD measures, respectively: NP 0.96 ± 0.013, 0.91 ± 0.028, p = .00002 GF 0.93 ± 0.020, 0.91 ± 0.022, p = .0035 MD 0.93 ± 0.021, 0.88 ± 0.027, p = .00002	Alperin et al. [8]
Segmentation Flood fill and morphology **Parameterization** Conic projection based on conic axis defined by lens center to center of vitreous body.	T1 3D inversion recovery turbo gradient echo: 0.5 mm in plane isotropic (FOV 40 x 46 mm); slice thickness, 1mm; TR, 2.5 ms; TE, 4.55 ms; flip angle, 16°; inversion time, 1280 ms;	Retinal distance map can be quantified by MRI * MRI vs optical biometry axial length mean ± SD difference: 0.08 ± 0.23 mm p = 0.01 * MRI retinal map reliability: SD = 0.11 mm (4 subjects, scanned twice) * Does not account for patient orientation changes	Beenakker et al. [24]
Segmentation Flood fill followed by spherical mesh shrink-wrap and local averaging. **Parameterization** Circumferential w.r.t axial length	T2 half-acquisition turbo spin-echo sequence: 0.5 mm place isotropic (FOV, 256 x 256 mm); 1 mm slice thickness; TR, 1240 ms; TE, 124 ms; flip angle, 150°; 6 averages; 4/8 partial-phase acquisition	Axial length can be quantified by MRI * Circumferential color-coding w.r.t axial length * Axial length intersession repeatability (one subject, 10 scans) mean ± SD: Right eye = 23.78 ± 0.27 mm Left = 24.41 ± 0.52 mm	Singh et al. [25]
Segmentation Intensity offset global thresholding **Parameterization** Iterative closest point registration; circumferential and meridional coordinate system.	T2 axial spin echo fat suppressed MRI: 0.390 mm in plane isotropic (FOV, 100 x 100); 0.800 mm slice thickness and spacing; TR, 750 ms; TE 111 ms; flip anlge, 170°; pixel bandwidth, 211 Hz/pixel .	Retinal changes unresolved after spaceflight. * 2D polar displacement map * Mean displacement moderately correlated with change in ocular biometry axial length: R^2 = 0.624. * Mean difference between change in ocular biometry axial length and mean displacement: 0.045 ± 0.124 mm. * Not dependent on patient orientation	Current study

Ocular biometric measurements are the gold standard for measuring anatomical characteristics of the eye[50], including the axial length. In the astronaut population, the difference between pre and postflight axial length provides a single value to quantify globe flattening. Axial length is a clinically accepted measurement against which our displacements can be compared, although the displacement parameter computed in our study is based on a different optical axis than axial length. Specifically, while axial length is measured along the optical axis of the eye (cornea to fovea), our displacement quantifies changes along an axis between the center of the lens and the location of the optic nerve head (roughly 4 mm from the fovea). Although this is slightly different to the axial length parameter, it does permit a valid comparison of changes in posterior globe shape.

The mechanisms underlying globe flattening are likely multifactorial and complex, e.g. orbital pressure may be altered in microgravity, yet this has not been investigated[25]. Since only a subset of astronauts develop clinically relevant globe flattening, there are likely individual-specific risk factors for globe flattening.

IIH is often discussed in the context of SANS because optic disc edema, ONS distention, and globe flattening are observed in both disorders. In IIH, these clinical features have been attributed to elevated ICP, and thus a decrease or reversal of the TLPD[39,51]. However, astronauts do not exhibit many of the other symptoms of IIH, including chronic headache, diplopia, and pulse synchronous tinnitus, and unlike the bilateral globe flattening associated with IIH, globe flattening associated with SANS can be asymmetric[19]. In the present study, the two subjects with the most significant globe flattening had flattening present in both eyes, although the degree of flattening was different in each eye (Figure 4.2 A). Further research is needed to elucidate any similarities in the etiologies of SANS and IIH.

Some limitations exist in this study, including the small number of astronaut subjects studied. The inherent challenges in MRI acquisition and segmentation can lead to artifacts in images of the cornea and lens, requiring subjective assessment of geometric agreement between point clouds. Despite these limitations, we have shown that our technique can detect and quantify volume displacement, and we are confident in the interpretability of our results. Although MRI techniques can be used to examine orbital anatomy, scanning is not feasible during spaceflight, restricting these types of studies to pre- and postflight assessment. Recovery likely begins immediately after return to Earth, and if so, our first MRI scan around 4 days after landing may not fully reflect inflight values.

The goal of this study was to develop and apply an automated non-invasive method to prospectively quantify posterior globe flattening in long-duration spaceflight astronauts, as well as the postflight recovery profile. A novel technique was developed and used to quantify posterior globe volume displacement from MRI scans in 10 astronauts after their respective ~6 month spaceflight missions, and at 5 recovery time points after spaceflight. The greatest degree of globe displacement was detected in our first postflight scan, and values gradually recovered with time after flight but were only partially resolved within one year. Further work is needed to fully understand the etiology of SANS, including the cause(s) of globe flattening. Application of the method in healthy subjects over time will help define the resolution of the method, and application of the method in more astronauts with who have participated in spaceflights of different durations will help identify the relationship between globe flattening and spaceflight duration, including extended missions up to one year.

Chapter 5: MRI-Based Quantification of Posterior Globe Flattening Resulting from Strict 6° Head-Down-Tilt Bed Rest, and the Effect of Daily Centrifugation

Abstract

Spaceflight is known to cause lasting health issues in humans, requiring countermeasures to reduce their effects. In particular, Spaceflight-Associated Neuro-ocular Syndrome (SANS) can causes reduced visual acuity in some long-duration spaceflight astronauts which is believed to be the result of structural ophthalmic abnormalities such as posterior globe flattening. A clearer diagnosis of SANS and a deeper understanding of ophthalmic abnormalities as a result of long-duration spaceflight are needed to help determine the feasibility of manned interplanetary expeditions.

Previous studies have hypothesized that a major contributor of SANS is a headward fluid shift that occurs in microgravity due to the loss of a hydrostatic pressure gradient. Head-down tilt (HDT) bed rest induces fluid shifts that are similar to those experienced during weightlessness and thus HDT has been proposed as an analog to microgravity. HDT studies allow for a better understanding of SANS pathophysiology and comprehensive testing of mitigation techniques.

In the present study, 24 healthy subjects were separated into three treatment groups and placed in strict 6° HDT bed rest for 60 days. Two of the groups received daily artificial gravity (AG) countermeasures in the form of continuous centrifugation for one group (cAG) and intermittent centrifugation for the other (iAG). The third group received no intervention (control). Magnetic resonance images (MRI) were collected and an automated non-invasive

method was applied to quantify posterior globe volume displacement during and immediately after HDT bed rest, when compared to baseline

On average, all groups displayed increased globe flattening with longer HDT duration with no significant differences observed between groups. The findings of this study suggest that strict HDT bed rest provides a reasonable analog to microgravity and that the mitigation techniques used may not significantly reduce the severity of SANS.

Introduction

SANS overview

Ophthalmic structural and functional changes in a condition known as Spaceflight-Associated Neuro-ocular Syndrome (SANS) have been observed in astronauts after long-duration spaceflight (> 6 months)[2,19,48,52]. The proportion of astronauts who are diagnosed with SANS is about 40 percent, but varies over time due to the ongoing characterization of its formal designation [23]. Ophthalmic abnormalities associated with SANS include choroidal folds, optic disc edema, hyperopic shift, and posterior globe flattening (Figure 5.1)[23] and can cause reduced visual acuity and farsightedness. In some subjects, these changes have been shown to persist long after return to Earth[4,22]. Headward fluid shifts that occur in the absence of a hydrostatic pressure gradient in weightlessness are thought to be a primary contributor of SANS, leading to mild but chronic elevation in intracranial pressure (ICP) and reduced visual acuity[53]. Increases in ICP may result in a reversal of the trans-laminar pressure difference (TLPD), wherein ICP becomes greater than intraocular pressure (IOP), contributing to scleral flattening[13,25].

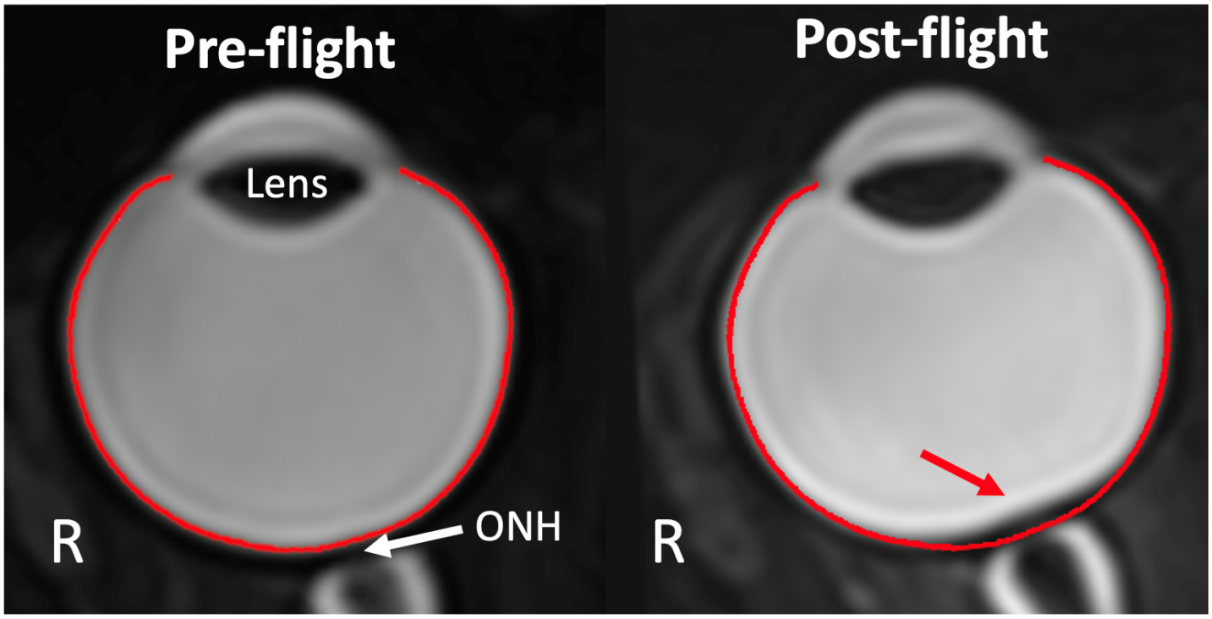

Figure 5.1. Posterior globe flattening has been identified subjectively and objectively after long-duration spaceflight and as a major symptom of SANS. A contour (red) is overlayed on a preflight and postflight T2-weighted MRIs to show globe flattening that occurred after long-duration spaceflight.

Spaceflight Analogs

Other well-known spaceflight-associated conditions, such as bone and muscle atrophy, have well defined etiologies and mitigation techniques. However, mitigation techniques for SANS are difficult to develop due to prohibitive costs and limitations of inflight monitoring and countermeasure implementation. Spaceflight analogs have been proposed to simulate the effects of microgravity on Earth. Currently, head-down tilt (HDT) studies are used as a spaceflight analog because the HDT position simulates fluid redistributions that are suspected to occur in microgravity[9]. However, the presence of a constant gravitational vector during HDT may elicit different physiological responses compared to spaceflight.

HDT Studies

Previous studies have tested HDT angles ranging from 4° to 15+°, but 6° is the most common because it reproduces approximately -0.1 G_z [54]. A subjective assessment of ground-based spaceflight analogs found that HDT showed good fidelity in simulating the effects of microgravity for fluid redistribution but not for neurologic and pulmonary function[10]. HDT studies have been shown to overestimate fluid redistributions compared to microgravity. One study found 45% of participants in a strict 6° HDT for 30 days developed optic disc edema, compared to 15% found in astronauts[55]. This suggests that ophthalmic changes may be more sensitive to HDT duration than spaceflight duration, allowing for shorter study durations.

Mitigation Techniques

The majority of spaceflight-associated conditions are attributed to the lack of a gravitational force in space. This has led researchers to test if replacing gravitational forces with centrifugal forces could mitigate the negative effects of weightlessness [56]. In short-term HDT studies, short-arm centrifugation was an effective countermeasure for musculoskeletal deconditioning[57] and orthostatic tolerance[58] in bed rest subjects. Both studies noted that intermittent centrifugation was more effective than continuous centrifugation in reducing the effects of HDT, and daily centrifugation is well tolerated by participants[59]. However, the effectiveness of centrifugation in mitigating the neuro-ocular effects of HDT and spaceflight has yet to be determined.

Study Aim

The aim of this study was to quantify volume displacement of the posterior ocular globe during and after 60-day HDT bed rest, and to assess the effectiveness of continuous and intermittent centrifugation as mitigation techniques (Figure 5.2). To accomplish this, an automated MRI-based method was applied to segment the optic globe and compare follow-up posterior globe shapes to baseline, pre-bedrest globe shape.

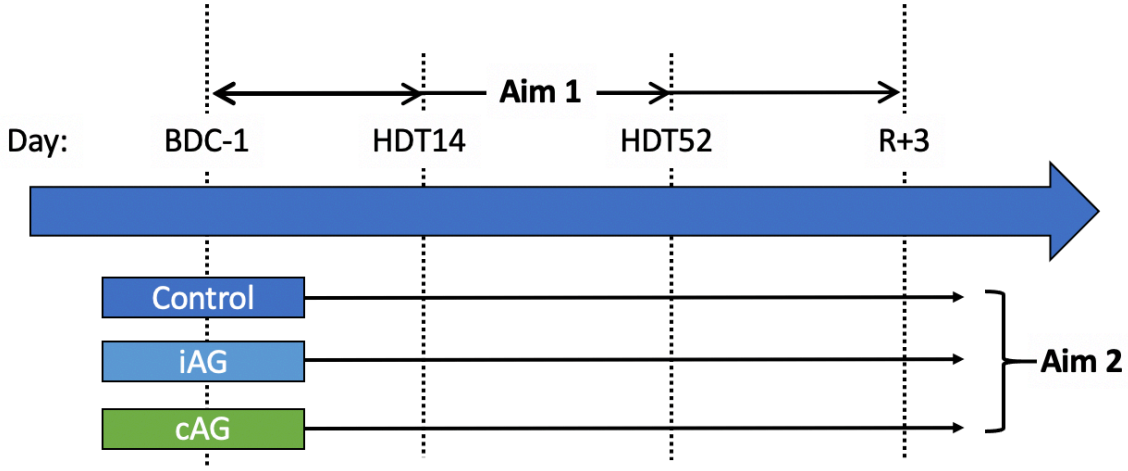

Figure 5.2. Schematic of summarizing the study design and study aims of the AGBRESA study. This figure was adapted from figure 2.1. Subjects were split into three study groups that participated in 60 days of strict, 6° HDT. Aim 1: posterior globe volume displacement compared to baseline (BDC-1) was measured at HDT day 14 (HDT14), HDT day 52 (HDT52) and at three days post-HDT (R+30). Aim 2: differences between the control and artificial gravity groups (iAG and cAG) were assessed to test the effect of centrifugation as a mitigation technique.

Methods

Study Design

In this randomized controlled study, subjects participated in a 60-day strict 6° HDT bed rest at the :envihab facility of the German Aerospace Center (DLR) in Cologne, Germany. MRI scans were collected at four timepoints throughout the study. Baseline scans were collected one day before bedrest (BDC-1), scans during bedrest were collected at 14 (HDT14) and 52

(HDT52) days, and follow-up scans were collected 3 days after bedrest (R+3). Researchers were blind to participants' subject groups and demographic information until after quantification of globe displacement was complete.

Participants

Written informed consent was obtained from all participants and was approved by the ethics committee of the Northern Rhine Medical Association (Ärztekammer Nordrhein, application #2018143) in Duesseldorf, Germany, as well as the Federal Office for Radiation Protection (Bundesamt für Strahlenschutz). 16 males and 8 females successfully completed the study, but two female subjects were omitted from the final data due to MRI artifacts. Subjects were randomly assigned to one of the following groups: the intermittent artificial gravity group (iAG, n = 7, 2 females, body mass index (BMI) 23.42 ± 1.57, age 35 ± 11 years), the continuous artificial gravity group (cAG, n = 8, 3 females, BMI 24.00 ± 1.71, age 32 ± 10 years), and the control group (ctrl, n =7, 1 female, BMI 25.39 ± 2.71, age 33 ±7 years) (Table 5.1).

Table 5.1. Table showing the number of subjects, sex, BMI, and age for the iAG, cAG and control study groups.

Group	Number of subjects	Sex	BMI (mean ± SD)	Age (Years) (mean ± SD)
iAG	7	5M, 2F	23.52 ± 1.57	34.86 ± 11.14
cAG	8	5M, 3F	24.00 ± 1.71	31.88 ± 9.75
Control	7	6M, 1F	25.39 ± 2.71	32.57 ± 6.75
All Subjects	22	16M, 6F	24.29 ± 2.13	33.04 ± 9.05

HDT Bedrest

Participants remained in a tightly controlled environment for a total of 89 days, including 29 days of acclimation and recovery, and the remaining 60 days spent in beds with the head tilted 6° below horizontal. During the 60 days of HDT, participants were required to keep one shoulder on the bed at all times and the use of pillows was not permitted to avoid confounding of results[53]. All daily activities including eating and hygiene were performed in the HDT position. Diet was strictly controlled throughout the study with a daily energy intake of 1.3 times the resting metabolic rate and daily water intake of 50 mL/kg body mass. Twenty-four-hour monitoring by trained staff ensured Young's modulus with all protocols.

Artificial Gravity

Participants in the artificial gravity (AG) groups completed daily sessions of centrifugation during the bed rest portion of the study. Gravity was simulated in the DLR short-arm centrifuge (Figure 5.3) which has a radius of 3.8 m and spun at a subject-specific rotational speed to achieve an acceleration of 1 g at the center of mass and 2 g at the feet and rotational direction alternated daily. The cAG group completed continuous 30-minute sessions while the iAG group completed six, five-minute bouts of centrifugation with three-minute breaks in between. Centrifugation occurred in the supine position (0° HDT) but subjects were positioned in 6° HDT immediately before and after each centrifuge run. Participants were instructed to gaze at a fixed point while on the centrifuge to avoid head movements. All AG sessions were carried out under the supervision of a medical doctor.

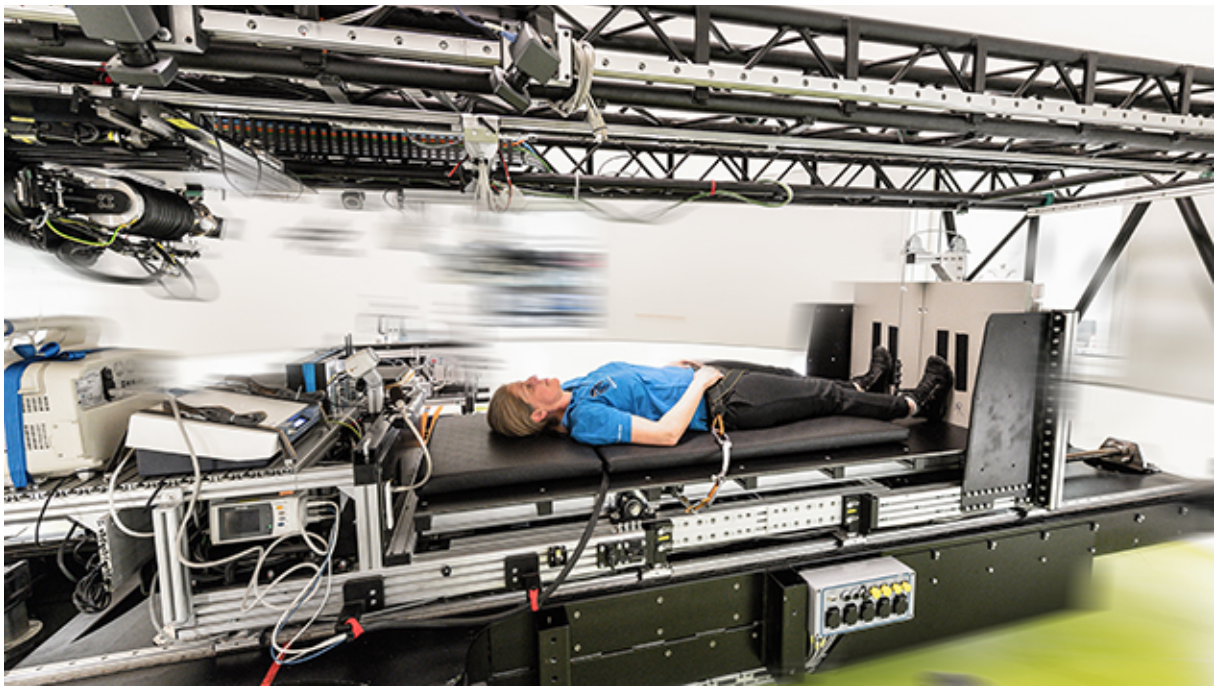

Figure 5.3. The Short Arm Human Centrifuge located at the :envihab research facility. The centrifuge has a radius of 3.8 m and spun at subject-specific rotational speed to generate an acceleration of 1 g at the center of mass and 2 g at the feet to simulate gravity for the iAG and cAG study groups. Image source: DLR (German Aerospace Center), Cologne, Germany.

MRI Acquisition and Reformatting

T2-weighted axial spin-echo fat-suppressed MRI sequences were collected using a 3T system with 0.78 mm in plane isotropic pixel size (FOV 100 x 100), and 0.78 mm slice thickness and spacing. Additional sequence parameters included a 170° flip angle, 750 ms repetition time, and 112 ms echo time.

Point Cloud Generation and Alignment

Each globe underwent an automated multistep 3D reconstruction and displacement mapping process in MATLAB (vers 2019a, Mathworks Corp. Natick, MA.) previously described by Sater et al. [60]. In brief, each globe was radial resliced about a central rotational axis at one-

degree increments in Osirix MD (vers. 8.0.1, Pixmeo, Geneva, Switzerland) (Figure 5.4 A). Segmentation of each slice was completed using an offset value of pixel intensity based on a global threshold to create a contour. Contours were transformed into 3D coordinates on a common axis to create a point cloud of the globe. A box grid filter was applied (MATLAB computer vision toolbox, pcdownsample) to ensure uniform point distribution. An iterative closest point registration algorithm with 60 iterations (MATLAB computer vision toolbox, pcregistericp) was applied to align follow up point clouds to their respective baseline (BDC-1) point clouds (Figure 5.1 B). The spherical coordinates of each point on the posterior hemisphere of the globe surface were expressed in a 2D polar coordinate distance map. Circumferential and meridional angles of each point were transformed into polar angles and radial locations, respectively, and the distance between of the points from the baseline point cloud's centroid was represented by a color on the distance maps. The baseline distance map was subtracted from the follow up distance map to generate a paired displacement map (Figure 5.4 C). Volume displacement was calculated for the region of the distance map within 4 mm of the optic nerve head (Figure 5.4 D).

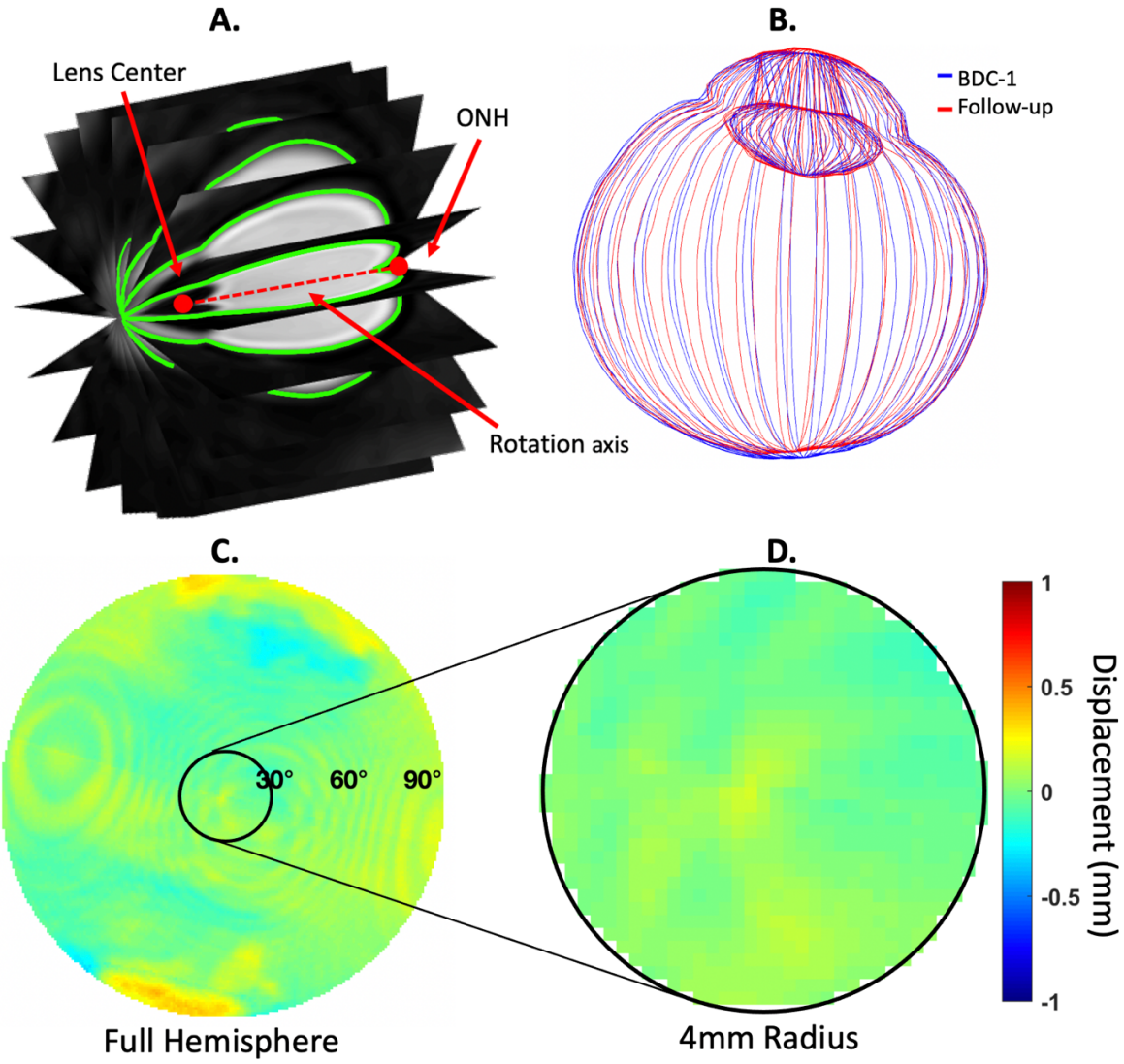

Figure 5.4. Methods for segmenting t2-weighted axial ocular MRI. A) Images were radially resliced and segmented. B) Baseline and follow-up globe point clouds were aligned using iterative closest point registration. C) Displacement maps of the posterior globe were generated for each baseline and follow-up pair. D) Posterior optic globe displacement was quantified for a region within a 4 mm radius of the ONH.

Statistics

A linear mixed-effects model that accounts for repeated measurements from the same individual was developed:

$$y_i = \beta_0 + \beta_1 x_{1i} + \beta_2 x_{2i} + \beta_3 x_{3i} + \beta_4 x_{4i} + \beta_5 x_{5i} + \beta_6 x_{6i} + z_{0i} + z_{1i} x_{2i} + z_{2i} x_{3i} + z_{3i} x_{4i} + \epsilon_i$$

Where y_i is the measurement of a parameter of interest, β_0 is the baseline (left eye of a male subject at BDC-1 and in the ctrl group), x_{1i} is the treatment group, x_{2i} is the timepoint, x_{3i} denotes the right eye, x_{4i}, x_{5i}, and x_{6i} are the age, sex, and BMI of the *i*th subject, respectively. While coefficient β represents fixed effect sizes and coefficient z represents the random effects.

The "*fitlme*" function in MATLAB (vers. R2019a Mathworks Corp., Natick, MA) was used to estimate the coefficients and variances in this linear mixed-effects model and test the hypotheses. This model appoints treatment group, timepoint, eye, age, BMI, and sex as fixed effects, with the corresponding coefficient indicating the effect size. This model treats the subjects as random with repeated measurements, which allows us to account for the variability across subjects and dependence between groups, timepoints, and eyes, for each subject. P-values for globe volume displacement were calculated with this linear-mixed effects model. We accounted for multiple comparison with Bonferroni correction in order to derive more conservative results.

Results

Posterior Globe Displacement by Duration

HDT duration results are summarized in Table 5.2. On average, posterior globe volume displacement increased with HDT duration, and did not recover within three days post-HDT for all three study groups (Figure 5.5). For the iAG group, average volume displacement was 2.44 mm^3 (95% CI -1.80 mm^3 to 6.84 mm^3, p = 0.252) at HDT14, 4.74 mm^3 (95% CI -0.59 mm^3 to 10.07 mm^3, p = 0.080) at HDT52, and 5.47 mm^3 (95% CI -0.12 mm^3 to 11.06 mm^3, p = 0.055)

at R+3 when compared to BDC-1 (baseline). For the cAG group, average displacement was 0.85 mm^3 (95% CI -2.59 mm^3 to 4.29 mm^3, $p = 0.620$) at HDT14, 5.05 mm^3 (95% CI 0.03 mm^3 to 10.07 mm^3, $p = 0.049$) at HDT52, and 4.23 mm^3 (95% CI 1.25 mm^3 to 7.22 mm^3, $p = 0.006$) at R+3 when compared to BDC-1. For the control group, average displacement was 1.00 mm^3 (95% CI -1.47 mm^3 to 3.47 mm^3, $p = 0.42$) at HDT14, 3.50 mm^3 (95% CI 0.76 mm^3 to 6.25 mm^3, $p = 0.013$) at HDT52, and 6.86 mm^3 (95% CI 2.96 mm^3 to 10.75 mm^3, $p = 0.001$) at R+3 when compared to BDC-1.

Effect of AG on Posterior Globe Volume Displacement

On average, AG groups had less volume displacement than the control group, but these differences were insignificant. The volume displacement for the iAG group on average was 0.17 mm^3 ($p = 0.942$) less than the control group and the displacement for the cAG group on average was 1.11 mm^3 ($p = 0.633$) less than the control group (Figure 5.5 A).

Demographic Effects and Unilaterality

Demographics and differences between eyes were assessed to see if any of the changes were associated with demographic effects or unilaterality. Age was associated with an increase in volume displacement of 0.21 mm^3 (95% CI 0.10 mm^3 to 0.32 mm^3, $p = 0.0001$). On average, females had 8.21 mm^3 more volume displacement than males (95% CI 5.82 mm^3 to 10.59 mm^3, $p < 0.0001$) (Figure 5.5 B). Differences between eyes and all other demographic effects were insignificant.

Table 5.2. Table showing the mean and standard error (SE) of posterior globe volume displacement at HDT day 14 (HDT14), HDT day 52 (HDT52) and at three days post-HDT (R+30) for the iAG, cAG and control study groups.

Group	HDT14 (mean ± SE, mm^3)	HDT52 (mean ± SE, mm^3)	R+3 (mean ± SE, mm^3)
iAG	2.44 ± 2.10	4.74 ± 2.64	5.47 ± 2.77
cAG	0.85 ± 1.71	5.05 ± 2.50 *	4.23 ± 4.49 **
Control	1.00 ± 1.22	3.51 ± 1.36 *	6.86 ± 1.93 ***

note: $p < 0.05$, $p < 0.01$**, $p < 0.001$****

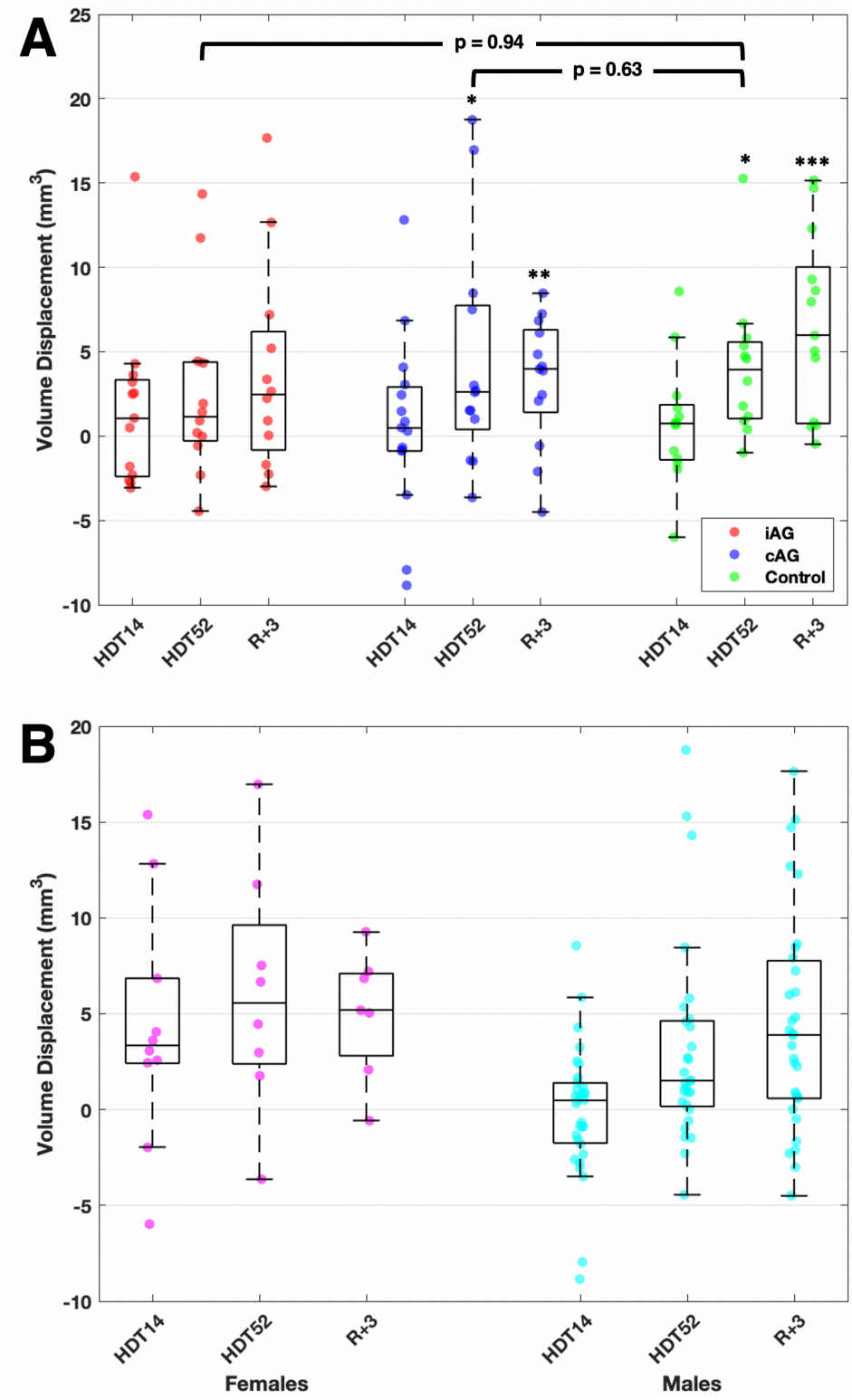

Figure 5.5. A) Plot showing volume displacement for the iAG (red), cAG (green) and control groups (blue) at HDT14, HDT52, and R+3 with statistical significance shown ($p<0.05$ *, $p<0.01$ **, $p<0.005$ ***). B) Plot showing the distribution volume displacement for males (cyan) and females (magenta) at all three timepoints. All displacements are referenced pre-HDT baseline geometries.

Discussion

Non-invasive automated techniques were applied to MRIs of HDT bed rest participants to quantify posterior optic globe volume displacement over time and assess the effectiveness of centrifugation as a mitigation technique. Small, inward displacements of the peripapillary choroidal-scleral interface were found to increase with HDT duration, with no recovery within three days post-HDT. Neither continuous nor intermittent centrifugation were significantly effective in reducing these displacements. Women were found to have greater posterior globe volume displacement when compared to men and older age was also associated with increased displacement.

The methods used in this study segmented the optic globe near the choroidal-scleral interface, and thus the displacements measured are likely due to a combination of scleral flattening, choroidal swelling, and retinal thickening. A previous study found that after 30 days of strict 6° HDT, total retinal thickness had increased by 53.9 µm and choroidal thickness remained unchanged[55]. This suggests that the volume displacements measured here are partially attributed to scleral flattening because they exceed that which could be explained by retinal thickening alone.

Scleral flattening is likely caused by a multitude of factors, but a reversal of the TLPD is suspected to play a role. Invasive measurements of ICP in rhesus monkeys during 6° HDT found that ICP immediately increased but slowly recovered to near supine levels over the course of 30 minutes[61]. If 6° HDT results in supine-level ICP, this pressure is still elevated beyond what has been measured in the seated or standing positions[53]. Chiquet et al. measured IOP over

seven days of 6° HDT and found that after an initial increase, IOP decreased from baseline by 0.96 mmHg after five days and 1.56 mmHg after seven days[62]. The combination of chronically elevated ICP to supine levels and reduced IOP creates a persistent reversal of the TLGP that may be causing the scleral flattening observed in the present study.

Significant globe volume displacement has been identified in astronauts using identical methods previously described. This supports the use of strict, long-term HDT bed rest studies as a ground-based analog to spaceflight. Average volume displacement in the astronaut cohort was 9.88 mm^3 approximately 4 days after returning from long-duration spaceflight (167 ± 17 days), far exceeding the displacements reported here[60]. The most probable explanation for the difference is the extended duration of spaceflight, but the presence of choroidal engorgement in astronauts likely played a contributing role.

Posterior globe volume displacement tended to increase with HDT duration. At HDT14, none of the study groups showed statistically significant displacement, which suggests that the sclera is somewhat resistant to perineural forces caused by changes in the TLPD. However, by R+3, volume displacement increased significantly, suggesting that long-term alterations in the TLPD can result in remodeling of scleral tissue. This may explain why globe flattening in astronauts is not resolved within a year after returning from space[60].

For most subjects, volume displacement increased between HDT52 and R+3. This timeframe included eight additional days of HDT and three days of acclimation and recovery. It is likely that displacement continued to increase during the additional eight days of bed rest, but it is expected these increases would be small relative to the previous 52 days. The increase in displacement observed between the last two time-points suggests that little recovery

occurred in the three days of acclimation. If recovery is insignificant within the first few days of acclimation, astronauts' posterior globes may be largely unchanged in days following return to Earth. Laurie et al. reported an average decrease of 12.7 µm in peripapillary total retinal thickness six days after a 30-day HDT study[55]. Displacements of this magnitude would be nearly undetectable by the methods described here.

Although differences between the AG groups and the control group were not statistically significant, the AG groups did have lower average volume displacements by R+3 when compared to the control group. Daily 30-minute centrifugation sessions may not be sufficient to significantly reduce globe flattening if mild but chronically elevated ICP is the cause. The typical adult will spend at least 16 hours per day in the upright position, during which time ICP is well below supine levels[53]. A 30-minute duration is only 3.1% of the time a typical adult spends in the upright position.

Sex was shown to be a contributing factor in posterior globe volume displacement. On average, females had significantly greater volume displacement at all three timepoints when compared to males (Figure 5.5 B). This is an interesting finding since idiopathic intracranial hypertension is much more common in females[63]. However, no female astronauts have been diagnosed with Frisèn grade edema, and Laurie et al. did not identify a difference between sexes in retinal thickening during 30-day HDT bed rest[55]. One study non-invasively estimated optic nerve sheath (ONS) stiffness using HDT and finite element modeling and found the ONS stiffness to be significantly greater in males[64]. If the ONS acts as a compensatory mechanism for ICP fluctuations [65], then a higher degree of displacement would be expected from subjects

with stiffer ONSs. Females were highly underrepresented in this study, warranting further investigation into the effect of sex in the development of SANS symptoms.

There are several limitations that remain unaddressed in this study. This study uses a novel method that needs to be validated for reliability and repeatability. However, previous applications of this method showed good agreement with ocular biometry measurements[60]. Another limitation is the low number of subjects in the study, particularly women. Finally, the duration of centrifugation was a small fraction of the typical time spent by an adult in a lowered ICP state.

These findings suggest that strict HDT studies provide an appropriate ground-based analog to spaceflight for studying mitigation techniques for posterior globe flattening. Daily 30-minute sessions of neither continuous centrifugation nor intermittent centrifugation were sufficient to significantly reduce the degree of globe volume displacement. Future studies with longer centrifuge duration may result in a more significant reduction in globe flattening. Significant differences between males and females warrant further investigation into the effect of sex on SANS-related ophthalmic alterations. Applying these methods in healthy subjects over time will help determine the repeatability of the methods and provide a measure of nominal changes in the posterior globe.

Chapter 6: Project Research Outputs

Below is a list of grants secured for or due to this project, and a record of abstracts and publications that were generated utilizing this research.

Grants Secured

Analysis and interpretation of ocular MRI sequences for the Artificial Gravity Bed Rest – European Space Agency (AGBRESA)

Source: NASA

Investigators: Martin BA (PI)

Goal: To determine how countermeasures applied during long-duration bedrest at envihab: facility impact ophthalmic and intracranial structural alterations.

Ophthalmic and intracranial structural changes in head-down tilt bedrest: potential countermeasures and comparison to SANS findings in astronauts (OPTICS study)

Source: NASA 80NSSC20K0920

Investigators: Martin BA (PI)

Goal: To determine if ophthalmic and intracranial structural alterations are similar in prolonged 6-degree HDT bed rest compared to long-duration astronauts with SANS, and determine if these alterations will be reduced by countermeasures applied during bed-rest.

Investigating structure and function of the eye

Source: NASA 17-BPBA_2-0024

Investigators: Macias B (PI), Martin BA (co-I)

Goal: Identify if greater ocular alterations occur with increased astronaut flight duration

Changes of the optic nerve dura mater in astronauts and SANS (OPTIMA)

Source: NASA 18-18OMNI_2-0112

Investigators: Ethier R (PI), Martin BA (co-I)

Goal: Use image post-processing and modeling to quantify change to dura mater properties.

Investigating Long-term Structural and Functional Changes in the Eye and Brain after Spaceflight

Source: NASA

Investigators: Martin BA (PI)

Goal: Quantify eye changes in astronauts over many years post flight.

Expanded measurements of ophthalmic structural changes in astronauts (EXPAND)

Source: NASA

Investigators: Martin BA (PI)

Goal: Apply image-post processing to quantify eye changes in large astronaut cohort.

Ocular Biomechanics Assessment in Astronauts (Phase 2)

Source: KBR Wyle / NASA Prime Grant No. NNJ15HK11B

Investigators: Martin BA (PI)

Goals: Extend imaging techniques to quantify eye deformation in additional astronauts

Simulations of CSF, Hemodynamics and Ocular Risk (VIIP SCHOLAR)

Source: NASA, NNX16AT06G

Investigators: Ethier R (PI), Martin BA (Co-I, sub-award)

Goal: Develop tools to compute CSF fluid shifts in microgravity and the affect on the eye.

Ocular Biomechanics Assessment in Astronauts

Source: KBR Wyle / NASA Prime Grant No. NNJ15HK11B

Investigators: Martin BA (PI, sub-award from parent)

Goal: Apply imaging techniques to objectively quantify eye deformation over space flight.

Advanced Ocular and Brain MRI of Astronauts Following Long Duration Space Flight

Source: Idaho Space Grant Consortium, NASA Prime Grant No. NNX15AI04H

Investigators: Law J (PI), Martin BA (PI, sub-award from parent)

Goal: Develop tools to quantify optic nerve tortuosity and 3D structure.

Abstracts Published

A. Seiner, S. Sater, G. Conley Natividad, E. Bershad, A Fu, B.R. Macias, K. Marshall-Goebel, S. Laurie, B.A. Martin, "MRI-Based Quantification of Posterior Globe Flattening in Head-Down Tilt Bedrest Subjects, and the Effect of Centrifugation", 2021 NASA Human Research Program / IWS (Galveston, TX, January, 2021).

Marshall-Goebel K, Brunstetter T, Gibson C, Kramer L, Laurie SS, Lee SMC, Mader T, Martin BA, Otto C, Patel N, Ploutz-Snyder R, Riascos R, Rohr J, Samuels B, Sargsyan A, Sass A, Sater S, Stenger MB, Macias BR, "Quantification of Spaceflight-Induced Ocular Changes," Aerospace Medical Association Conference (Atlanta, GA, May 17-21, 2020).

Sater SH, Rohr JJ, Sass AM, Stenger MB, Macias BR, Ebert D, Sargsyan AE, Marshall Goebel K, Hargens A, Dulchavsky SA, Ploutz-Synder RJ, Martin BA, "Magnetic Resonance Imaging Quantification of Ophthalmic Changes Due to Spaceflight" Hydrocephalus Society Meeting (Vancouver, Canada, 9/13-16, 2019).

Lee C, Rohr JJ, Sass A, Sater S, Martin BA, Zahid A, Oshinski J, Ethier CR, "In Vivo Estimation of Optic Nerve Sheath Stiffness Using Noninvasive MRI Measurements and Finite Element Modeling," Summer Bioengineering, Biotransport, and Biomechanics Conference, SB3C (Seven Springs, PA, 6/25-28, 2019).

Martin BA, Rohr J, Sass A, Sater S, Macias B, Stenger M, “Magnetic Resonance Imaging Quantification Of Opthalmic Changes Due To Space Flight,” 2019 NASA Human Research Program / IWS (Galveston, TX, January 23, 2019).

Rohr JJ, Sass AM, Sater S, Macias B, Oshinski JN, Ethier CR, Stenger M, Martin BA, “MRI-based quantification of optic nerve tortuosity and subarachnoid space 3d geometry: reliability assessment,” NASA Human Research Investigator’s Workshop (Galveston, TX, 1/22-25/2018).

Rohr JJ, Sass AM, Stenger M, Macias B, Ethier CR, Sargsyan AE, Martin BA, “Automated Method to Quantify 3D Geometric Alterations of the Optic Nerve and Sheath in Astronauts,” NASA Human Research Program Investigators’ Workshop, The Gateway to Mars (Galveston, TX, 1/22-25, 2018).

Sass AM, Sater S, Rohr JJ, Macias B, Oshinski JN, Ethier CR, Stenger M, Martin BA, “Methods for Quantifying Tortuosity and 3D Geometry Changes Occurring to the Optic Nerve During Long-Duration Spaceflight,” University of Idaho Undergraduate Research Symposium (Moscow, ID, 4/30, 2018).

Rohr JJ, Sass AM, Sater S, Aldrimk B, Stenger M, Macias B, Ethier CR, Sargsyan A, Martin BA, “Inter-operator Reliability Assessment of Optic Nerve Tortuosity in Long-duration Flight Astronauts,” 33rd Annual Meeting of the American Society for Gravitational and Space Research (Seattle, WA, 10/25-28/2017).

Sater S, Sass A, Aldrimk B, Rohr JJ, Stenger M, Macias B, Martin BA, “Reliability assessment of Optic Nerve Trajectory in Long-duration Space Flight Astronauts,” University of Idaho, Undergraduate Student Research Symposium (Moscow, ID, 4/24, 2017).

Submitted Publications

Sater, S. *et al. “Automated MRI-Based Quantification of Posterior Ocular Globe Flattening and Recovery After Long-Duration Spaceflight”* Submitted for review (2020).

Sater, S. et al. *“MRI Based Quantification of Ophthalmic Changes in Healthy Volunteers During Acute 15° Head-Down Tilt as an Analog to Microgravity”* Submitted for review (2020).

Peer-Reviewed Publications

Rohr JJ, Sater S, Sass AM, Marshall-Goebel K, Ploutz-Snyder RJ, Ethier CR, Stenger MB, Martin BA, Macias BR (2020), "*Quantitative magnetic resonance image assessment of the optic nerve and surrounding sheath after spaceflight*." NPJ Microgravity, 6: 30. https://doi.org/10.1038/s41526-020-00119-3

Lee C, Rohr J, Sass A, Sater S, Zahid A, Macias B, Stenger MB, Samuels BC, Martin BA, Oshinski JN, Ethier CR (2020), "*In vivo estimation of optic nerve sheath stiffness using noninvasive MRI measurements and finite element modeling*." Journal of the Mechanical Behavior of Biomedical Materials, 110: 103924.

Chapter 7: Conclusion

Several overarching conclusions were made from the research reported here:

- Acute HDT resulted in ONS distension that was significantly greater than what has been previously measured in astronauts.
- Long-duration spaceflight was associated with significant posterior globe flattening
- Posterior globe flattening did not resolve within one year after return from long-duration spaceflight.
- Strict HDT bed rest proves an effective strategy for simulating the ophthalmic effects of spaceflight and testing countermeasures.
- Strict 60-day HDT bedrest resulted in significant posterior globe flattening that was not sufficiently mitigated with 30 minutes of daily centrifugation.

Future work

Currently, the reliability and repeatability of the globe segmentation methods are unknown. A longitudinal study assessing posterior volume displacement in healthy subjects will help define the repeatability of the method and provide information about how the geometry of the posterior globe naturally changes over time. Additional countermeasures such as LBNP, thigh cuff, and vitamin B supplement should be attempted in future HDT studies with the methods reported here applied to assess their efficacy in reducing globe flattening. Other variables such as exercise should also be tested to see if they contribute to globe flattening. Applying these methods to more astronauts, particularly female astronauts, will help further our understanding of SANS physiology and demographic contributors to globe flattening in SANS and IIH.

References

1 (ed Human Research Program) (https://humanresearchroadmap.nasa.gov/intro/, 2008).

2 Lee, A. G., Mader, T. H., Gibson, C. R., Brunstetter, T. J. & Tarver, W. J. Space flight-associated neuro-ocular syndrome (SANS). *Eye (Lond)* **32**, 1164-1167, doi:10.1038/s41433-018-0070-y (2018).

3 Zhang, L. F. & Hargens, A. R. Spaceflight-Induced Intracranial Hypertension and Visual Impairment: Pathophysiology and Countermeasures. *Physiol Rev* **98**, 59-87, doi:10.1152/physrev.00017.2016 (2018).

4 Mader, T. H. *et al.* Persistent Globe Flattening in Astronauts following Long-Duration Spaceflight. *Neuro-Ophthalmology*, 1-7, doi:10.1080/01658107.2020.1791189 (2020).

5 Hargens, A. R. & Vico, L. Long-duration bed rest as an analog to microgravity. *J Appl Physiol (1985)* **120**, 891-903, doi:10.1152/japplphysiol.00935.2015 (2016).

6 Mader, T. H. *et al.* An overview of spaceflight-associated neuro-ocular syndrome (SANS). *Neurol India* **67**, S206-S211, doi:10.4103/0028-3886.259126 (2019).

7 Rohr, J. J. *et al.* Quantitative magnetic resonance image assessment of the optic nerve and surrounding sheath after spaceflight. *NPJ Microgravity* **6**, 30, doi:10.1038/s41526-020-00119-3 (2020).

8 Laurie, S. S. *et al.* Optic Disc Edema and Choroidal Engorgement in Astronauts During Spaceflight and Individuals Exposed to Bed Rest. *JAMA Ophthalmol* **138**, 165-172, doi:10.1001/jamaophthalmol.2019.5261 (2020).

9 Watenpaugh, D. E. Analogs of microgravity: head-down tilt and water immersion. *J Appl Physiol (1985)* **120**, 904-914, doi:10.1152/japplphysiol.00986.2015 (2016).

10 Schneider, S. M. *et al.* Treadmill exercise within lower body negative pressure protects leg lean tissue mass and extensor strength and endurance during bed rest. *Physiol Rep* **4**, doi:10.14814/phy2.12892 (2016).

11 Lee, C. *et al.* In vivo estimation of optic nerve sheath stiffness using noninvasive MRI measurements and finite element modeling. *Journal of the Mechanical Behavior of Biomedical Materials* **110**, doi:10.1016/j.jmbbm.2020.103924 (2020).

12 Patel, N., Pass, A., Mason, S., Gibson, C. R. & Otto, C. Optical Coherence Tomography Analysis of the Optic Nerve Head and Surrounding Structures in Long-Duration International Space Station Astronauts. *JAMA Ophthalmol* **136**, 193-200, doi:10.1001/jamaophthalmol.2017.6226 (2018).

13 Johannesson, G., Eklund, A. & Linden, C. Intracranial and Intraocular Pressure at the Lamina Cribrosa: Gradient Effects. *Curr Neurol Neurosci Rep* **18**, 25, doi:10.1007/s11910-018-0831-9 (2018).

14 Kramer, L. A., Sargsyan, A. E., Hasan, K. M., Polk, J. D. & Hamilton, D. R. Orbital and intracranial effects of microgravity: findings at 3-T MR imaging. *Radiology* **263**, 819-827, doi:10.1148/radiol.12111986 (2012).

15 R.S. Johnston, L. F. D. Biomedical Results from Skylab. (National Aeronautics and Space Administration, Washington D.C., 1977).

16 Hargens, A. R., Bhattacharya, R. & Schneider, S. M. Space physiology VI: exercise, artificial gravity, and countermeasure development for prolonged space flight. *Eur J Appl Physiol* **113**, 2183-2192, doi:10.1007/s00421-012-2523-5 (2013).

17 Tanaka, K., Nishimura, N. & Kawai, Y. Adaptation to microgravity, deconditioning, and countermeasures. *J Physiol Sci* **67**, 271-281, doi:10.1007/s12576-016-0514-8 (2017).

18 Adrian LeBlanc, C. L., Linda Shackelford, Valentine Sinitsyn, Harlan Evans, Oleg Belichenko, Boris Schenkman, Inessa Kozlovskaya, Victor Oganov, Alexi Bakulin, Thomas Hedrick, and Daniel Feeback. Muscle volume, MRI relaxation times (T2), and body composition after spaceflight. *Journal of Applied Pysiology* **86**, 6 (200).

19 Mader, T. H. *et al.* Optic disc edema, globe flattening, choroidal folds, and hyperopic shifts observed in astronauts after long-duration space flight. *Ophthalmology* **118**, 2058-2069, doi:10.1016/j.ophtha.2011.06.021 (2011).

20 Mader, T. H. *et al.* Persistent Asymmetric Optic Disc Swelling After Long-Duration Space Flight: Implications for Pathogenesis. *J Neuroophthalmol* **37**, 133-139, doi:10.1097/WNO.0000000000000467 (2017).

21 Laurie, S. S. *et al.* Optic Disc Edema and Choroidal Engorgement in Astronauts During Spaceflight and Individuals Exposed to Bed Rest. *JAMA Ophthalmol*, doi:10.1001/jamaophthalmol.2019.5261 (2019).

22 Macias, B. R. *et al.* Association of Long-Duration Spaceflight With Anterior and Posterior Ocular Structure Changes in Astronauts and Their Recovery. *JAMA Ophthalmol*, doi:10.1001/jamaophthalmol.2020.0673 (2020).

23 Lee, A. G. *et al.* Spaceflight associated neuro-ocular syndrome (SANS) and the neuro-ophthalmologic effects of microgravity: a review and an update. *NPJ Microgravity* **6**, 7, doi:10.1038/s41526-020-0097-9 (2020).

24 Chen, L. M. *et al.* Ultrasonic measurement of optic nerve sheath diameter: a non-invasive surrogate approach for dynamic, real-time evaluation of intracranial pressure. *Br J Ophthalmol* **103**, 437-441, doi:10.1136/bjophthalmol-2018-312934 (2019).

25 Marshall-Goebel, K. *et al.* Intracranial and Intraocular Pressure During Various Degrees of Head-Down Tilt. *Aerosp Med Hum Perform* **88**, 10-16, doi:10.3357/AMHP.4653.2017 (2017).

26 Daboul, A. *et al.* Reproducibility of Frankfort horizontal plane on 3D multi-planar reconstructed MR images. *PLoS One* **7**, e48281, doi:10.1371/journal.pone.0048281 (2012).

27 Buck, A. H. *A Reference Handbook of the Medical Sciences: Embracing the Entire Range of Scientific and Practical Medicine and Allied Science*. Vol. 5 (W. Wood & Company, 1894).

28 Magnaes, B. Body position and cerebrospinal fluid pressure *J. Neurosurg.* **44**, 7 (1976).

29 Killer, H. E., Laeng, H. R., Flammer, J. & Groscurth, P. Architecture of arachnoid trabeculae, pillars, and septa in the subarachnoid space of the human optic nerve: anatomy and clinical considerations. *Br J Ophthalmol* **87**, 777-781 (2003).

30 Xiaobin Xie , X. Z., Jidi Fu , Huaizhou Wang , Jost B Jonas , Xiaoxia Peng , Guohong Tian ,Junfang Xian , Robert Ritch , Lei Li , Zefeng Kang , Shoukang Zhang , Diya Yang , Ningli Wang. Noninvasive intracranial pressure estimation by orbital subarachnoid space measurement *Critical Care* **17**, 12 (2013).

31 Wostyn, P. & De Deyn, P. P. Optic Nerve Sheath Distention as a Protective Mechanism Against the Visual Impairment and Intracranial Pressure Syndrome in Astronauts. *Invest Ophthalmol Vis Sci* **58**, 4601-4602, doi:10.1167/iovs.17-22600 (2017).

32 Wang, X. *et al.* Finite Element Analysis Predicts Large Optic Nerve Head Strains During Horizontal Eye Movements. *Invest Ophthalmol Vis Sci* **57**, 2452-2462, doi:10.1167/iovs.15-18986 (2016).

33 Raykin, J. *et al.* Characterization of the mechanical behavior of the optic nerve sheath and its role in spaceflight-induced ophthalmic changes. *Biomech Model Mechanobiol* **16**, 33-43, doi:10.1007/s10237-016-0800-7 (2017).

34 Wahlin, A. *et al.* Optic nerve length before and after spaceflight. *Ophthalmology*, doi:10.1016/j.ophtha.2020.07.007 (2020).

35 Lanny C. Keil, K. H. M., Michael G. Skidmore, John Hines, Walter B. Severs. The effect of head-down tilt and water immersion on intracranial pressure in nonhuman primates. *Aviation, Space, and Environmental Medicine* **63**, 5 (1992).

36 Kiel LC, M. K., Skidmore MG, Hines J, Severs WB. The effect of head-down tilt and water immersion on intracranial pressure in nonhuman primates. *Aviat Space Environ Med*, 181-185 (1992).

37 Marshall-Goebel, K. *et al.* Assessment of Jugular Venous Blood Flow Stasis and Thrombosis During Spaceflight. *JAMA Netw Open* **2**, e1915011, doi:10.1001/jamanetworkopen.2019.15011 (2019).

38 Alperin, N., Bagci, A. M., Lam, B. L. & Sklar, E. Automated quantitation of the posterior scleral flattening and optic nerve protrusion by MRI in idiopathic intracranial hypertension. *AJNR Am J Neuroradiol* **34**, 2354-2359, doi:10.3174/ajnr.A3600 (2013).

39 Jacobson, D. M. Intracranial hypertension and the syndrome of acquired hyperopia with choroidal folds. *J Neuroophthalmol* **15**, 178-185 (1995).

40 Hingwala, D. R., Kesavadas, C., Thomas, B., Kapilamoorthy, T. R. & Sarma, P. S. Imaging signs in idiopathic intracranial hypertension: Are these signs seen in secondary intracranial hypertension too? *Ann Indian Acad Neurol* **16**, 229-233, doi:10.4103/0972-2327.112476 (2013).

41 Friedman, D. I. Idiopathic intracranial hypertension. *Curr Pain Headache Rep* **11**, 62-68 (2007).

42 Cheng, H. *et al.* Structural and functional MRI reveals multiple retinal layers. *Proc Natl Acad Sci U S A* **103**, 17525-17530, doi:10.1073/pnas.0605790103 (2006).

43 Duong, T. Q. Magnetic resonance imaging of the retina: from mice to men. *Magn Reson Med* **71**, 1526-1530, doi:10.1002/mrm.24797 (2014).

44 Shen, Q. *et al.* Magnetic resonance imaging of tissue and vascular layers in the cat retina. *J Magn Reson Imaging* **23**, 465-472, doi:10.1002/jmri.20549 (2006).

45 Grytz, R. *et al.* Material properties of the posterior human sclera. *J Mech Behav Biomed Mater* **29**, 602-617, doi:10.1016/j.jmbbm.2013.03.027 (2014).

46 Azhdam, A. M., Goldberg, R. A. & Ugradar, S. In Vivo Measurement of the Human Vitreous Chamber Volume Using Computed Tomography Imaging of 100 Eyes. *Translational Vision Science & Technology* **9**, doi:10.1167/tvst.9.1.2 (2020).

47 Macias, B. R. *et al.* Association of Long-Duration Spaceflight With Anterior and Posterior Ocular Structure Changes in Astronauts and Their Recovery. *JAMA Ophthalmol* **138**, 553-559, doi:10.1001/jamaophthalmol.2020.0673 (2020).

48 Mader, T. H. *et al.* Optic disc edema in an astronaut after repeat long-duration space flight. *J Neuroophthalmol* **33**, 249-255, doi:10.1097/WNO.0b013e31829b41a6 (2013).

49 Jinkins, J. R. *et al.* MR of optic papilla protrusion in patients with high intracranial pressure. *AJNR Am J Neuroradiol* **17**, 665-668 (1996).

50 Chia, T. M. T., Nguyen, M. T. & Jung, H. C. Comparison of optical biometry versus ultrasound biometry in cases with borderline signal-to-noise ratio. *Clin Ophthalmol* **12**, 1757-1762, doi:10.2147/OPTH.S170301 (2018).

51 Wall, M. Idiopathic intracranial hypertension. *Neurol Clin* **28**, 593-617, doi:10.1016/j.ncl.2010.03.003 (2010).

52 Marshall-Goebel, K. *et al.* Lower body negative pressure reduces optic nerve sheath diameter during head-down tilt. *J Appl Physiol (1985)* **123**, 1139-1144, doi:10.1152/japplphysiol.00256.2017 (2017).

53 Lawley, J. S. *et al.* Effect of gravity and microgravity on intracranial pressure. *J Physiol* **595**, 2115-2127, doi:10.1113/JP273557 (2017).

54 Nelson, E. S., Myers, J. G., Jr., Lewandowski, B. E., Ethier, C. R. & Samuels, B. C. Acute effects of posture on intraocular pressure. *PLoS One* **15**, e0226915, doi:10.1371/journal.pone.0226915 (2020).

55 Laurie, S. S. *et al.* Optic Disc Edema after 30 Days of Strict Head-down Tilt Bed Rest. *Ophthalmology* **126**, 467-468, doi:10.1016/j.ophtha.2018.09.042 (2019).

56 Bukley A., P. W., Clément G. . Physics of Artificial Gravity. *Artificial Gravity. The Space Technology Library* **20**, doi:https://doi.org/10.1007/0-387-70714-X_2 (2007).

57 Rittweger, J. *et al.* Short-arm centrifugation as a partially effective musculoskeletal countermeasure during 5-day head-down tilt bed rest--results from the BRAG1 study. *Eur J Appl Physiol* **115**, 1233-1244, doi:10.1007/s00421-015-3120-1 (2015).

58 Linnarsson, D. *et al.* Effects of an artificial gravity countermeasure on orthostatic tolerance, blood volumes and aerobic power after short-term bed rest (BR-AG1). *J Appl Physiol (1985)* **118**, 29-35, doi:10.1152/japplphysiol.00061.2014 (2015).

59 Frett, T. *et al.* Tolerability of daily intermittent or continuous short-arm centrifugation during 60-day 6o head down bed rest (AGBRESA study). *PLoS One* **15**, e0239228, doi:10.1371/journal.pone.0239228 (2020).

60 Sater, S. *et al.* Automated MRI-Based Quantification of Posterior Ocular Globe Flattening and Recovery After Long-Duration Spaceflight. *Submitted for review* (2020).

61 Keil, L. C., McKeever, K. H., Skidmore, M. G., Hines, J. & Severs, W. B. The effect of head-down tilt and water immersion on intracranial pressure in nonhuman primates. *Aviat Space Environ Med* **63**, 181-185 (1992).

62 Chiquet, C. *et al.* Changes in intraocular pressure during prolonged (7-day) head-down tilt bedrest. *J Glaucoma* **12**, 204-208, doi:10.1097/00061198-200306000-00004 (2003).

63 Durcan, F. J., Corbett, J. J. & Wall, M. The incidence of pseudotumor cerebri. Population studies in Iowa and Louisiana. *Arch Neurol* **45**, 875-877, doi:10.1001/archneur.1988.00520320065016 (1988).

64 Lee, C. *et al.* In vivo estimation of optic nerve sheath stiffness using noninvasive MRI measurements and finite element modeling. *J Mech Behav Biomed Mater* **110**, 103924, doi:10.1016/j.jmbbm.2020.103924 (2020).

65 Wostyn, P., Mader, T. H., Gibson, C. R. & Killer, H. E. The escape of retrobulbar cerebrospinal fluid in the astronaut's eye: mission impossible? *Eye (Lond)*, doi:10.1038/s41433-019-0453-8 (2019).